Università degli Studi di Padova

Dipartimento di Fisica e Astronomia "G. Galilei"
Laurea magistrale in Astronomia

tesi magistrale

Multiple Stellar Populations in Magellanic Clouds Clusters: disentangling between age spread and rotation

Relatore:
Prof. Antonino P. Milone

Correlatore:
Dr. Anna F. Marino

Laureando:
Giacomo Cordoni
Matricola: 1155711

21 Giugno 2018
Anno Accademico 2017/2018

Università degli Studi di Padova

Dipartimento di Fisica e Astronomia "G. Galilei"
Laurea magistrale in Astronomia

tesi magistrale

Multiple Stellar Populations in Magellanic Clouds Clusters: disentangling between age spread and rotation

Relatore:
Prof. Antonino P. Milone .....

Correlatore:
Dr. Anna F. Marino .....

Laureando:
Giacomo Cordoni .....

Anno Accademico 2017/2018

Contents

List of Figures

Abstract

The color-magnitude diagrams (CMDs) of all the old Globular Clusters (GCs) host multiple sequences, which correspond to stellar populations with different chemical composition and, possibly, different ages. Their origin is one of the most-intriguing open issues of stellar astrophysics and would provide new constraints on the assembly of the Galaxy and on the re-ionization of the Universe.
The recent discovery of multiple main sequences (MSs) and extended main-sequence turn offs (eMSTOs) in the CMDs of young and intermediate-age clusters of both Magellanic Clouds has suggested that multiple populations are not a peculiarity of old GCs. Indeed the most-straightforward explanation of the eMSTOs is that young clusters have experienced a prolonged star formation in close analogy with what has been suggested for old Galactic GCs. In this case, the young clusters of the Large and Small Magellanic Clouds (LMC, SMC) would provide the unique opportunity to investigate the multiple-population phenomenon a few hundreds Myrs after their formation. An alternative interpretation of the complex features observed in the CMD of these clusters sees star rotation as responsible for the eMSTOs and the split MSs. In this case, intermediate-age MC clusters would be formed from a single star-formation episode.
In this thesis I exploited HST archive data to disentangle the effects of age and rotation and constrain the origin of the eMSTO. I first reduced and analyzed HST images of the LMC cluster KMHK 250 and of the SMC cluster NGC 265, which have never been investigated in the context of multiple populations. I discovered that both clusters exhibit the eMSTO and that NGC 265 shows a split MS. The fact that KMHK250 is a very-low mass clusters suggests that the presence of the eMSTO does not depend on the cluster mass.
In addition, I analyzed the photometric catalogs of 27 young and intermediate-age clusters from the HST survey of multiple populations in Magellanic-Clouds clusters. I find that if an age spread is considered the responsible for the eMSTOs, the resulting age spreads strongly correlate with the cluster age. The comparison between the observed CMDs and simulated CMDs derived from Geneva models show that such correlation is due to stellar populations with different rotation rates.
I conclude that there is no evidence for large age spread within young and intermediate-age Magellanic-Cloud clusters and that any internal age variation, if present, is smaller than 100 Myrs.

CHAPTER 1

Introduction

1.1 Multiple Stellar Populations in Globular Clusters

The presence of more than one stellar population in GCs is the most fascinating and enigmatic discovery in the field of stellar populations in the last years. The definition itself of a GC as the prototype of a Simple Stellar Population (SSP), definitively shattered out. Based on the SSP assumption, GCs have served as laboratory for stellar evolution as stars in a given GC were assumed coeval and chemically homogeneous. One of the direct consequences of the failure of the SSP assumption is that stellar evolutionary models, which use GCs as calibrators, need to be updated. Furthermore, the properties of stellar populations in these ancient stellar systems provide important information on the Universe at its earliest phases, including the primordial pre-enrichment of the interstellar medium by the first stars and the role of first galaxies in the assembly of the halo.
It seems that multiple stellar populations are not a peculiarity of the old Galactic GCs. Indeed, thanks to our HST survey on Magellanic Clouds clusters, we have discovered that the CMDs of young (age 50-500 Myr) GCs in both Magellanic Clouds exhibit split main sequences (MS) and extended MS turn-offs. Intermediate-age GCs in the Magellanic Clouds show similar eMSTO. Despite a huge effort has been undertaken to understand these observations, the physical mechanism responsible for the eMSTO is still obscure. It has been suggested that it is due to coeval stellar populations with different rotation rates but it seems that rotation alone is not able to reproduce the observations. Several authors have suggested that the eMSTO is due to an age spread of 50-500 Myrs and that the clusters with the eMSTO are the younger counterparts of the old globular clusters with multiple populations. Potentially, if this idea will be confirmed observationally, the value of such a discovery in stellar astrophysics may correspond to the discovery of a still-alive dinosaur in paleontology.
In this thesis I present the contribution on the photometric analysis of multiple stellar populations in young and intermediate-age star clusters in the MCs. In this chapter the observational scenario, both for old Milky Way and young Magellanic Clouds GCs, is summarized, together with a brief description of the possible scenarios proposed to explain the presence of multiple populations in these objects.

1.1.1 Observations of Multiple Populations

GCs are among the oldest systems in our Galaxy, they are among the most studied objects in the universe. However, we still struggle understanding how they formed, and

why they are so common around every kind of galaxy, from giant elliptical galaxies to dwarf galaxies.
GCs were considered as the best prototype of simple populations born in a single star-formation episode, with the same age and same chemical composition.
For these reasons they were considered the perfect laboratory for testing stellar formation and evolution theory.
In the last decades, however, thanks to the improvements of the quality of observations, because of both better instruments (i.e. Hubble Space Telescope) and techniques, the widely accepted notion of GCs as constituted by a SSP has been challenged.
Photometric diagrams made with appropriate combinations of ultraviolet, optical and near-infrared filters are efficient tools to identify MPs in GCs. As an example, in the panels (a) and (b) of Figure 1.1.1 we show the m_{F814W} vs. $m_{F275W} - m_{F814W}$ CMD and the m_{F814W} vs.$C_{F275W,F336W,F438W}$ pseudo-CMD of the GC NGC 6723, which reveals multiple populations along the RGB and the MS of this cluster. The $\Delta_{CF275W,F336W,F438W}$ vs. $\Delta_{F275W,F814W}$ pseudo two-colors diagram, or 'Chromosome Map' is another efficient tool to separate stellar populations (see [Milone et al., 2015b] for details). As an example, panels (c) and (d) of Figure 1.1.1 show the chromosome map of RGB in NGC 6723 and the corresponding Hess diagram.

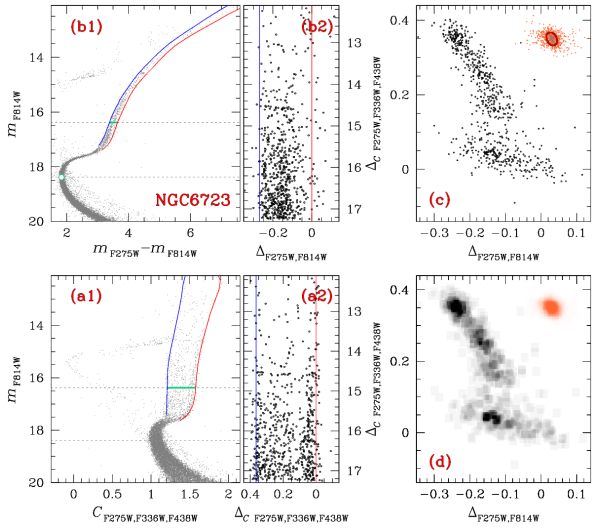

Figure 1.1.1: This Figure, taken from[Milone et al., 2016c], illustrates the procedure to derive the $\Delta_{F275W,F336W,F438W}$ vs. $\Delta_{F275W,F814W}$ pseudo two-color diagram (or "chromosome map") for the prototypical cluster NGC 6723. Panels (a1) and (b1) show the the m_{F814W} vs. $C_{F275W,F336W,F438W}$ pseudo-CMD and the m_{F814W} vs. $m_{F275W} - m_{F814W}$ CMD of NGC 6723. The "verticalized" m_{F814W} vs. $\Delta_{CF275W,F336W,F438W}$ and m_{F814W} vs. $\Delta_{F275W,F814W}$ diagrams for RGB stars are plotted in panels (a2) and (b2), respectively. Panel (d) shows the Hess diagram for stars in panel (c).

Of course, since the discovery of multiple sequences in the CMD of GCs, one of the biggest goal of modern astronomy has been that of explaining how these stars formed. According to the most-intriguing scenario, there is a first generation of stars, namely 1G, which pollutes the inter-stellar medium (ISM) where sequent generations (2G) form.
In general the first generation has a chemical composition similar to that of the cloud from which the cluster has formed, and the second generation is composed of stars depleted in Carbon (C) and Oxygen (O), but it is enriched in Sodium (Na), Nitrogen (N) and Helium (He). The abundances of light elements of GC stars define correlations and anti-correlations. As an example, the Na-O anti-correlations for RGB stars in the globular cluster M 4 is shown in Figure 1.1.2.

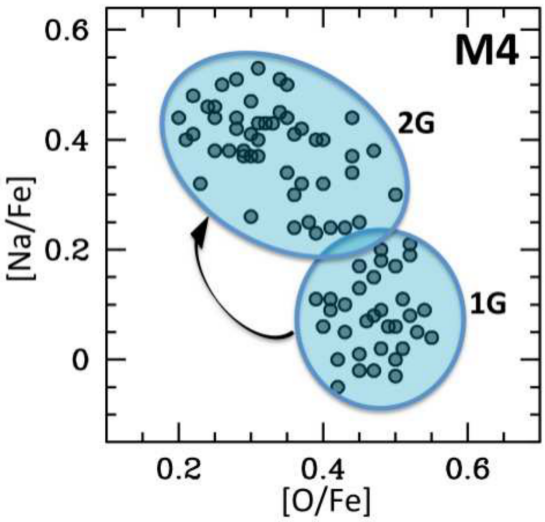

Figure 1.1.2: Na-O anti-correlations in the Galactic Globular Cluster M4

All the chemical patterns typical of the presence of distinct stellar populations in GCs translate into multiple photometric sequences along the CMD, allowing the analysis of the multiple stellar populations phenomenon for millions of stars from the MS up to the RGB and more advanced stages of stellar evolution. In recent years "*The Hubble Space Telescope UV Legacy Survey of Galactic Globular Cluster* (GO-13297, PI: G.Piotto, Piotto et al. 2015) has proven that multiple stellar populations are a common feature among all GCs, and has added constraints on the morphology of the second generation of stars. The main features characterizing the multiple stellar populations phenomenon can be summarized as follows:

- **GC Specificity** The presence of 2G stars, with their chemical features, although common to all GCs, is very rare in the Milky Way field. This suggests that these stars are very likely to form inside GCs. This means that every scenario which attempts modeling the formation of multiple stellar populations has to account for the rarity of 2G-like stars in the field, or in other words, has to be specific for GCs.

- **Ubiquity** As said before, multiple stellar populations are observed in almost every studied GC. This means that the formation of 2G stars is not a rare event that take place under particular circumstance, but it has to be a direct consequence of the formation of the GC itself.

- **Variety** While every GC host multiple populations, their features are quite different from case to case. We observe GCs with a number of populations that goes from a minimum of 2, up to a maximum of 17 and possibly more, and, each of them has its own peculiar chemical composition.

- **Predominance** 2G stars are, in most GCs, the dominant component, especially in the cluster center, where they account for more than the 50% of the stars.

- **Discreteness** Within each cluster multiple populations can be separated in quite distinct sequences in CMD and/or in two-color diagram. The same goes for chemical abundances, although in many cases it is more complex to distinguish between different stellar groups or clumps because of measurement errors in the chemical abundances. [Marino et al., 2008] and [Yong et al., 2005] proved for the first time the discreteness of the sequences using high resolution data.

- **Supernova avoidance** With some exceptions, 2G stars share the same metallicity

with 1G stars. This means that GCs have retained a really small fraction of SN products, and thus there is small contamination from these products in 2G stars.

- **Hot CNO and Ne-Na processing** A distinctive feature of 2G stars is the chemical composition that results from CNO-cycling and p-capture processes at high temperatures. Thus, every scenario should quantitatively account for the variety of composition patterns exhibited by 2G stars in all GCs that have been studied.

- **Helium enrichment** Almost every studied GC presents He-enriched 2G stars. Thus, 1G polluters have to account for producing/ejecting helium-rich material.

- **Mass Budget** One of the challenges for every scenario is the predominance of 2G stars, because only a small fraction of initial 1G stars mass ejected has the required chemical composition. A straightforward solution is to postulate that GC initial mass was much greater than the present-day mass. This means that GC progenitors have lost 80-90% of their masses.

1.1.2 Scenarios for the Formation of Multiple Populations

To interpret the observations, it has been suggested that soon after formation, some GC stars acted as polluters of the intra-cluster medium from which successive stellar generation(s) formed. In this scenario, GCs have experienced multiple bursts of star formation. Alternatively, the variations in light elements could be due to early-disk accretion in pre-main sequence binaries, rather than to multiple generations. Following this idea, the observed multiple stellar populations are coeval. So far, none of the scenarios proposed to explain the multiple stellar populations phenomenon fully meet all the observational constraints.
In brief, the most acknowledged polluters that have been proposed in the multiple stellar generations scenario are :

- **Asymptotic Giant Branch stars (AGB)** proposed originally by [Cottrell and Da Costa, 1981], this scenario was developed by the [D'Ercole et al., 2010] and [Ventura et al., 2001]. Intermediate mass AGB stars (3-4 $\lesssim \mathcal{M}/\mathcal{M}_{\odot} \lesssim 8$) are interested by peculiar nucleosynthesis processes, such as slow neutron capture (s-processes) and hot-bottom burning (HBB) which allows efficient p-capture nuclear processing. The elements produced in these processes are then injected in the ISM by stellar winds and subsequent evolution phases.
  In this scenario the fact that stars in a wide range of stellar masses contribute to the material which forms 2G stars ensures that p-processing takes place over a wide range of temperatures, with e.g., sodium being mostly provided by lower mass stars and oxygen-depleted material by the more massive ones.
  So, this model predicts a first episode of star formation leading to the 1G population, and a second one, when enough AGB ejecta has accumulated in the potential well of the cluster, after a few hundred Myrs. Then the cluster evolves, losing most of 1G stars via tidal interaction with the Milky Way. This model is able to reproduce some of the chemical patterns observed in GCs. A major shortcoming is that a Na-O correlation, instead of an anti-correlation, is expected.

- **Fast rotating massive stars** ($20\mathcal{M}_{\odot}$ and $\sim 100\mathcal{M}_{\odot}$). Because of rotations the nuclear burning products are mixed from the core to the envelope, and are then ejected in the ISM. This material then falls in the potential well of the cluster, and it is incorporated in 2G stars, resulting in stellar populations with an age difference of few tens Myrs. However, if this process occurs in nature, then it would not be specific of GC, and we would observe 2G stars in the Galactic-halo field, but we do not.

Furthermore in this scenario the distribution of chemical abundances is expected to be continuous, and not discrete.

- **Super massive stars (SMS)** [Denissenkov and Hartwick, 2013] and [Denissenkov et al., 2015] proposed the idea that stars in the center of the cluster would sink together forming SMS of about $10^4 \mathcal{M}_\odot$. A star of this mass would be fully convective, and would lose mass at a really high rate, enriching the ISM. Its wind, because of convection, which makes the star homogeneous, would be progressively enriched in helium and in products of CNO cycling and p-capture reactions, thus creating the chemical composition observed in 2G stars. Although fascinating, this model fails to fulfill some of the requirements, as for example SN avoidance, mass budget and Helium enrichment constraints.

In the idea of a lack of multiple star-formation episode :

- **Massive interacting binaries (MIB)** In a binary system, the forced rotation of the primary star envelope would cause mixing, which, if reaching down to the hydrogen-burning shell, would result in CNO and p-capture processing of the whole envelope, hence leading to helium enhancement, oxygen depletion, etc. Then, the processed envelope would enrich the ISM in the subsequent common-envelope phase of the MIBs. Within this scenario 2G stars can form directly out of the MIB ejecta [De Mink et al., 2009]; or these eject would be caught up by circumstellar disks of young low mass stars, which finally accrete it themselves.
  This model, like the previous one, presents some contradictions with observations. While GCs specificity is fulfilled, and variety might be, populations discreteness is a major problem, because large and random star-to-star differences in the amount of swept/accreted material is expected, thus preventing the formation of discrete populations. Also SN avoidance is an unfulfilled constraint.

Concluding, if the presence of multiple stellar populations is a well-established fact today, we are still far from understanding how GCs and multi populations formed. Finding age spreads between the different stellar populations would help discriminating between the two main ideas proposed to explain multiple populations.

1.2 Multiple Populations in Young and Intermediate-age Clusters

Similarly to Milky Way GCs, also young (YC) and intermediate-age (IAC) clusters were thought to be composed by a SSP. However, in the last years, extending our knowledge to Magellanic Cloud (MC) clusters with young ($< 1 Gyr$) and/or intermediate-age ($1 - 2 Gyr$), both in the Large Magellanic Cloud (LMC) and Small Magellanic Cloud (SMC) we provided strong evidence that their CMDs where not consistent with single isochrones, as expected in the case of a simple population.
Because of their relatively young age, if compared with the $\sim$ 11-13 Gyr old Galactic GCs, these systems offer us the unique possibility of disentangling stellar populations even with a few tens of Myr age difference.

1.2.1 Intermediate-age Clusters

[Bertelli et al., 2003], for the first time, suggested a prolonged star formation episode, spanning a range of $\sim 300 Myr$ for NGC 2173 in the LMC (see also [Mackey and Broby Nielsen, 2007] and [Baume et al., 2007]). Later on [Milone et al., 2009] proved that the presence of multiple stellar populations in clusters with age between 1 Gyr and 3 Gyr is a very common feature. In particular, these clusters display an extended Main Sequence Turn Off (eMSTO), whose color spread is much larger than what

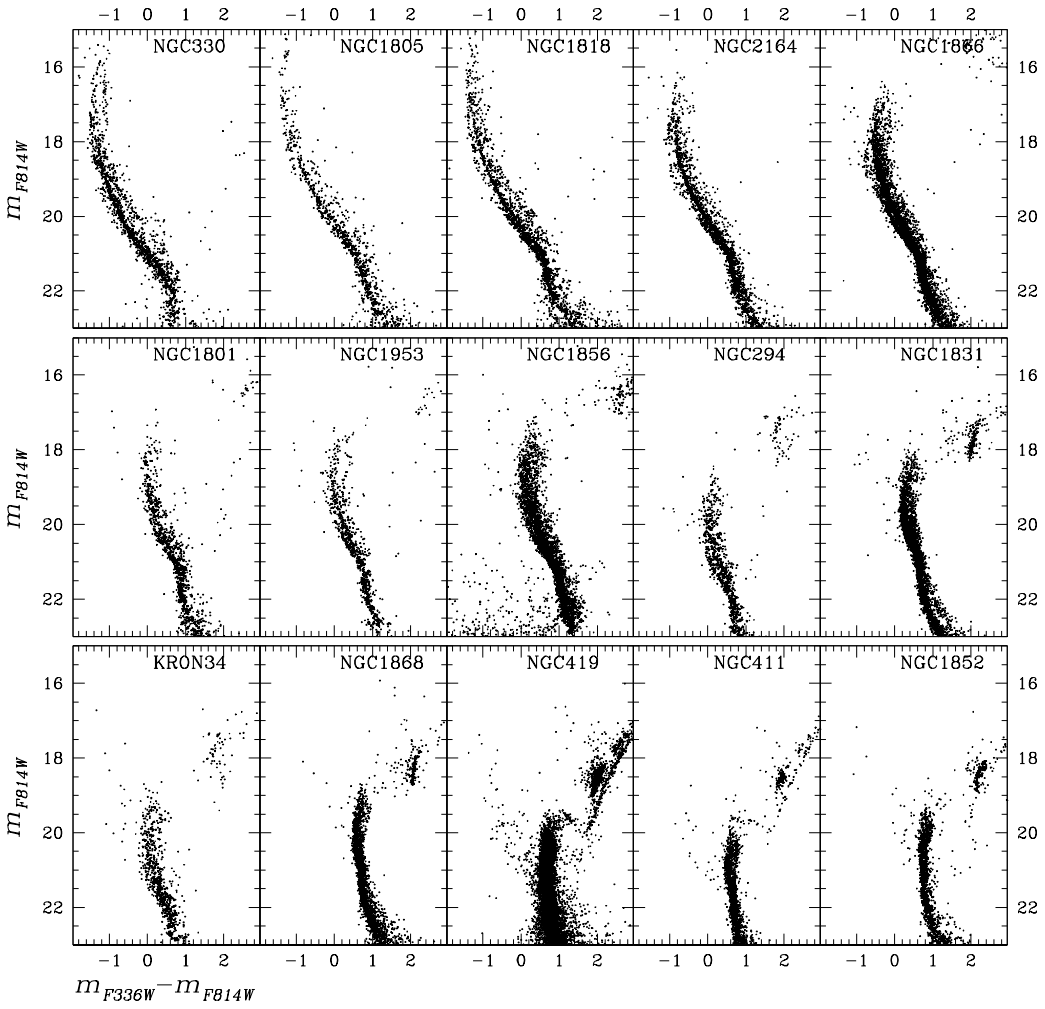

Figure 1.2.1: Collection of CMDs analyzed in this work. Only 15 out of 27 clusters are shown.

is expected from photometric errors alone, differential reddening or field contamination. The possibility that the same physical process is responsible for MPs in both young Magellanic Clusters and in old GCs, would provide a better understanding of old GCs. The question here is :

Are these clusters the young counterpart of old Galactic cluster with multipopulations? Do they really host multiple stellar generations?

If this is the case, then they could be a priceless source of information, allowing us to study multipopulations just a few years after their formation, improving our understanding of this phenomenon.
However, [Mucciarelli et al., 2011] and [Martocchia et al., 2018] found no evidence of star-to-star chemical abundances variation, which instead is a signature of the presence of MPs in old GGCs. This means that, chemical abundances variations, if present, are

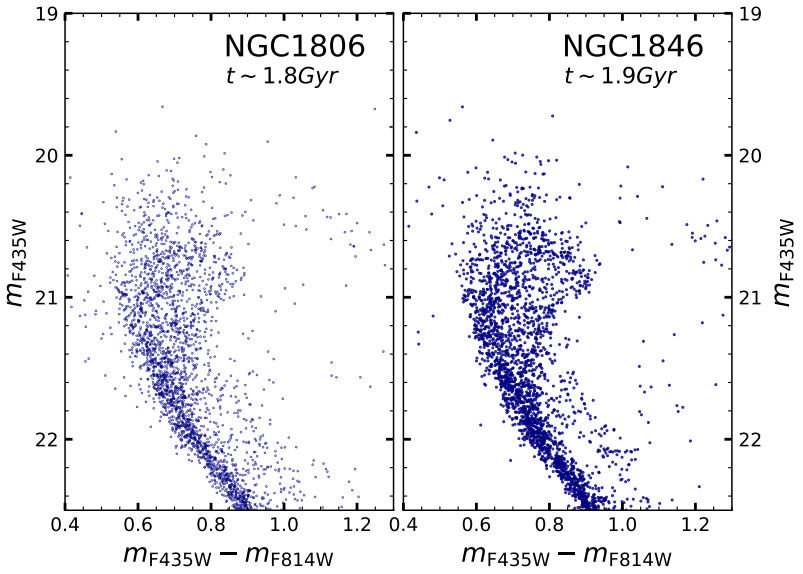

Figure 1.2.2: $m_{\rm F435W}$ vs. $m_{\rm F435W} - m_{\rm F814W}$ CMDs zoomed around the eMSTO of the intermediate-age LMC clusters NGC 1806 (age=1.8 Gyrs, left) and NGC 1846 (age=1.9 Gyrs, right).

lower than our instrumental threshold, and therefore can not be detected. This is still an important piece of information that adds-up to the multipopulations puzzle, but is far from being a conclusive proof.
The eMSTO observed in most IACs has been interpreted either with a spread in age of 100-500 $Myrs$ between stars in the same cluster and/or with different rotational velocities. If indeed the eMSTO is caused by age variations, then the cluster would indeed host multiple stellar generations. However for a cluster to host multiple star formation episodes, it is necessary to retain ejecta from a previous stellar generation which pollutes the gas from which the second generation can form, therefore its progenitor has to have a minimum mass of about $10^6 M_{\odot}$ at the time of the cluster formation.
In the latter scenario instead, rotation would affects star evolutionary lifetime, the morphology of the evolutionary tracks and the effective temperature that we see, which becomes function of the viewing angle because of temperature gradients
[Bastian and De Mink, 2009]. Briefly, the centrifugal acceleration reduces the effective gravity resulting in cooler and slightly less luminous stars. However, rotation also induces internal mixing processes, which can have the opposite effect, leading to more luminous and hotter stars. Which of these contrasting effects dominates depends on the initial mass, rotational velocity, and chemical composition. Thus, in the rotational scenario, there is no need to introduce multiple stellar populations with different age to reproduce the observed CMDs of IACs.

1.2.2 Young clusters

[Milone et al., 2015a] found that the young cluster NGC 1856 ($\sim 300Myr$) exhibit, in addition to an eMSTO, also a split MS. Specifically they observed a red MS (rMS) and a less populated blue one (bMS). The discovery of a split MS in young GCs provides a new perspective to investigate the multiple populations phenomenon in younger clusters. Comparison of the CMD of young clusters with isochrones seems to suggest that the split MS is best reproduced by two coeval stellar populations with distinct rotation: a

non-rotating population that hosts about 25% of MS stars and corresponds to the blue MS, and a population of red MS stars with rotational velocity close to the critical value [Milone et al., 2016a]. On the other hand, it is not clear yet if, in addition to rotation, age spread gives some contribution to the eMSTO observed in these objects.
One of the most debated argument in recent years has been that of disentangling between these two models, which we will refer to as the *age spread scenario* and the *rotational scenario*. In this thesis I will investigate this phenomenon, trying to shed light on this fascinating topic.

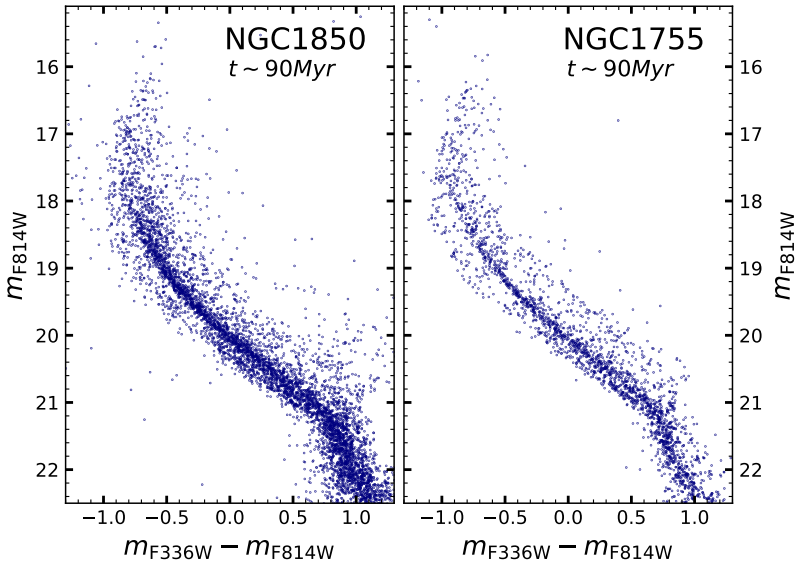

Figure 1.2.3: $m_{\rm F336W}$ vs. $m_{\rm F336W} - m_{\rm F814W}$ CMDs of the young LMC clusters NGC 1850 (age=90 $Myrs$, left) and NGC 1755 (age=90 $Myrs$, right). Note the split MS and the eMSTO.

1.2.3 *Age spread* Scenario

According to the age-spread scenario, Magellanic Magellanic Clouds clusters (MCCs) host multiple stellar populations with an age spread of up to several 10^8 years. Obviously, for a second star formation episode to happen, we need enough gas. And where does this gas come from? So far, three mechanisms have been suggested :

- mergers of young clusters with giant molecular clouds
- accretion of ambient gas by the clusters
- retention of stellar ejecta in the potential well of the clusters

Particularly, the last possibility requires the cluster to have a high enough mass to retain SN and stellar winds ejecta. If this is the case, we expect to find some sort of correlation between age spread and cluster mass .
[Goudfrooij et al., 2014] investigated this possibility studying a sample of 18 IACs, finding a correlation between MSTO width and central escape velocity for intermediate-age clusters, the latter quantifying the capability of the cluster to retain and/or accrete stellar ejecta. In particular the central escape velocity should be higher than the velocity of stellar winds of intermediate mass ($4 < \mathcal{M}/\mathcal{M}_{\odot} < 8$) AGB stars, which is $\sim 12-15 km/s$. This correlation is true for both cluster present-day mass, and the mass of the cluster

at $10Myr$ age, which is model-depending. This correlation would be easily verified or rejected studying the MSTO of an extreme low-mass clusters.
We show the results obtained in [Goudfrooij et al., 2014] in Figure 1.2.4. In particular they found that a cluster has to have a minimum mass of $log(\mathcal{M}_{cl}/\mathcal{M}_{\odot}) \sim 4.8$ at the age of $10Myr$ in order to retain/accrete the gas needed to ignite a second episode of stellar formation.

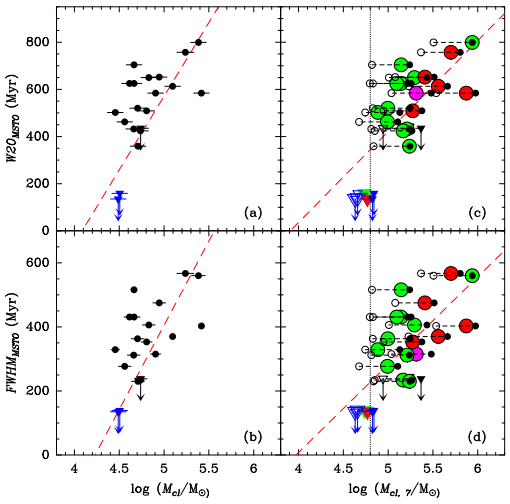

Figure 1.2.4: Age spread versus cluster mass at present age on the left, and at an age of 10 Myr. The Figure is taken from [Goudfrooij et al., 2014]. The dotted vertical line in the right panels is the lower mass limit for a cluster to host multiple star formation episodes $\log(M/M_{\odot})$.

The fact that, so far, there is no spectroscopic evidence of C, N, O, Na variations seems a challenge for this scenario. As a final consideration we add that, as explained in [Goudfrooij et al., 2014], if intermediate mass AGB stars are the main source of enriched material from which the second generation form, then the second formation episode would not start until $\sim$ 100-150Myr after the formation of the cluster. This is in contradiction with the recent findings by [Milone et al., 2015a], [Milone et al., 2016a] and [Milone et al., 2016b] of YCs with eMSTO and split MS, if interpreted as age spread.

1.2.4 *Rotational* Scenario

The "rotational" scenario, first introduced in [Bastian and De Mink, 2009], is an alternative interpretation of split MSs and eMSTOs.
As said before, rotation would affect the evolution of a star increasing the MS lifetime and modifying its physical parameters like temperature and luminosity, hence color and magnitude. In particular a rotating star, due to the different centrifugal force across its surface, tends to assume an oblate shape, deviating from its original spherical shape. As a consequence, the star develops a polar temperature gradient, with its maximum being at the poles. The shape and temperature structure introduce the viewing angle as an additional parameter. The photometry resulting from the "edge-on" configuration is then different from the "face-on" configuration. Therefore in our model we have to include both limb and gravity darkening effects. In this context, [Brandt and Huang, 2015] found that the extension of the MSTO region, computed like the area enclosed by the rotating isochrone and the non-rotating one, in mag^2, is proportional to the cluster age, peaking for ages $\sim$ 1-1.5Gyr and then decreasing, due to convection effects.

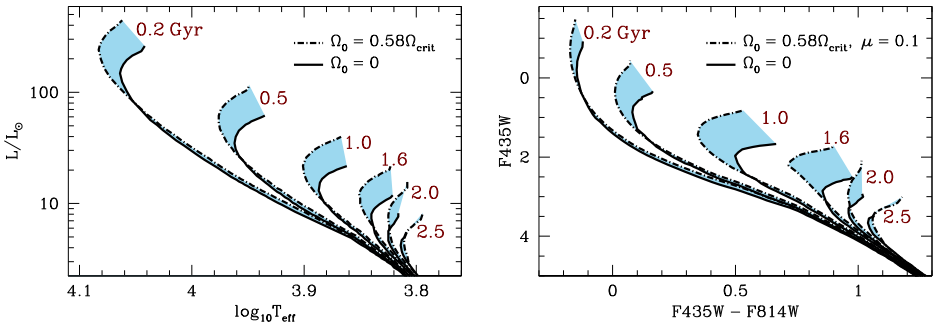

Figure 1.2.5: Effect of rotation on the Turn-Off region in Young Clusters and Intermediate-age Clusters, taken from [Brandt and Huang, 2015].

As we can see from Figure 1.2.5, clusters with ages up to $\sim 2Gyr$ show an eMSTO, its width peaking between 1-1.5Gyr. At ages greater than the $2Gyr$ limit, turnoff stars develop outer convective envelope while still on the MS and shed their angular momentum still young.

Therefore different rotation rates could theoretically explain the eMSTO in intermediate-age clusters. However in younger clusters we observe in addition to an eMSTO a split MS, with a blue MS hosting non-rotating or slowly rotating stars, and a red MS, with fast rotators. This feature further increases the complexity of the Magellanic Clouds multipopulations puzzle. [Milone et al., 2016a] investigates both eMSTO and split MS in the young cluster NGC1755, trying to determine whether the CMD is compatible with the age spread scenario or not.

Figure 1.2.6: Different CMDs of the SMC cluster NGC 330. Highlighted in red are Be stars, detected using the H_α photometry (right panel).

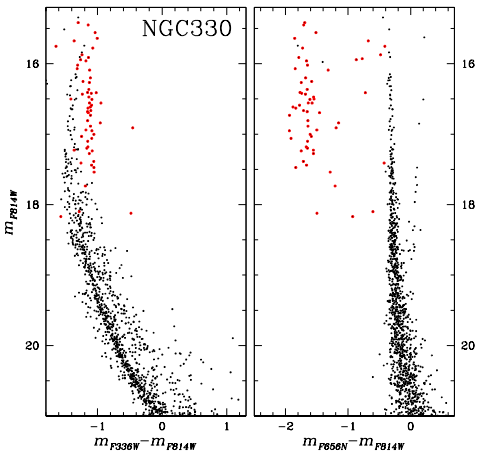

The results, at least for NGC1755, proved that the split MS was not in agreement with a simple physical age spread, even introducing different metallicity and Helium content between the two populations, while the CMD was well fitted by two populations with different rotation velocity, but same age and chemical abundances. In particular, to correctly reproduce the double MS, 75% of stars should be rapid rotators, with almost a critical/break-up angular velocity, while the remaining stars should be non-rotators. In the case of populations with different rotation, we know from theoretical models that slowly rotating stars on the bMS should evolve toward a shallower turn off luminosity than rotating stars, and this could explain part of the observed spread in the TO region.

As a conclusive remark on NGC1755, which is the first documented young cluster with split MS and eMSTO, together with NGC1856, we add that, according to the age spread model, it is expected not to host an eMSTO nor a split MS. [Goudfrooij et al., 2014] found in fact that the threshold mass for a cluster to have have more star formation episodes is $M_{cl} \sim 10^{4.8} M_\odot$, while NGC1755 has a mass of $M_{NGC1755} \sim 10^4 M_\odot$, well below this limit. According to this model, this cluster, with an age of approximately $80Myr$, should have had a mass greater of at least an order of magnitude, and somehow

lost it in this short time. We can not a priori exclude this possibility, however, this fact tends to favor the rotational scenario.

We have now to understand why there are two distinct stellar populations with different rotational velocity. This arise two questions: the first one concerns the actual presence of fast rotators, which is required to reproduce the CMD, and the second one concerns the physical mechanism which lead to the bimodality in the rotational velocity.
Regarding the presence, or not, of fast rotators we can find the answers in [Milone et al., 2018], in which a large populations of Be stars is detected using the m_{F814W} vs. $m_{F656N} - m_{F814W}$ CMD, which discriminates H_α emission of Be stars. These stars populate the MSTO and the red MS, as in Figure (1.2.6), but they do not populate the blue MS, in agreement with this scenario.
As for the second question, one possibility is that stars are somehow braked during their life, and they lose their angular momentum. We refer to this possibility as *rotational evolution*.

Rotational evolution

[D'Antona et al., 2017] suggested a theory that could actually answer some questions, but at the same time creates new ones. In the rotational scenario, the first issue is whether stars are born with different rotational velocity, or they have undergone some processes which actually changed their velocity. It is believed that, giving the fact that stars in a cluster form out of the same cloud, at birth they are likely to share the same rotational velocity. Therefore it is likely to assume that stars are born with moreover the same angular velocity, and only later they loses part of their angular momentum. Some physical mechanisms is then responsible for the braking of cluster stars. Let's take now into consideration a typical CMD of a young cluster with split main sequence and eMSTO. In order to fit every stellar component with isochrones, we have to introduce at least three populations, in red, blue and orange in Figure (1.2.7):

- coeval rapidly rotating stars on the red MS
- coeval slowly/non rotating stars on the blue MS
- younger slowly/non rotating stars in the upper part of the bMS

We need to introduce a population which is 25% younger then the other two main populations, and it has to be non rotating in order to reproduce the brighter part of the bMS. In some clusters, like NGC1856 we also need an older populations to reproduce the fainter part of the eMSTO. But still, we do not understand the origin of this populations. In particular, the main question we have to answer is why all younger stars are non rotating, and why there are no younger rotating stars.
We start assuming that all stars are coeval, and they were born out of the same cloud, therefore with the same rotational velocity. Then, due to the braking process, some of these stars have been braked during very early stage, others have only been braked recently and others are still to be braked. According to these scheme, the younger population is not actually younger, but by means of some mechanism, it mimics a younger population.
Theoretical rotational models predicts that the evolution of the core mass M_{core} and central temperature (T_c) as a function of the core hydrogen content (X_c), is very similar for non-rotating and rotating tracks, and the main difference is the total time spent along the evolution, because, in rotating stars, the mixing process feeds the convective core with fresh hydrogen-rich matter and thus extends the main-sequence life at each given X_c.
If we suppose that internal layers are the first to brake, then the timescale of the process depends both on stellar mass and its evolutionary stage, so that braked stars, i.e. the blue main sequence, may be present in clusters over a wide range of ages, as we observe. In this model the envelope is the last to brake, and only after the envelope braking the

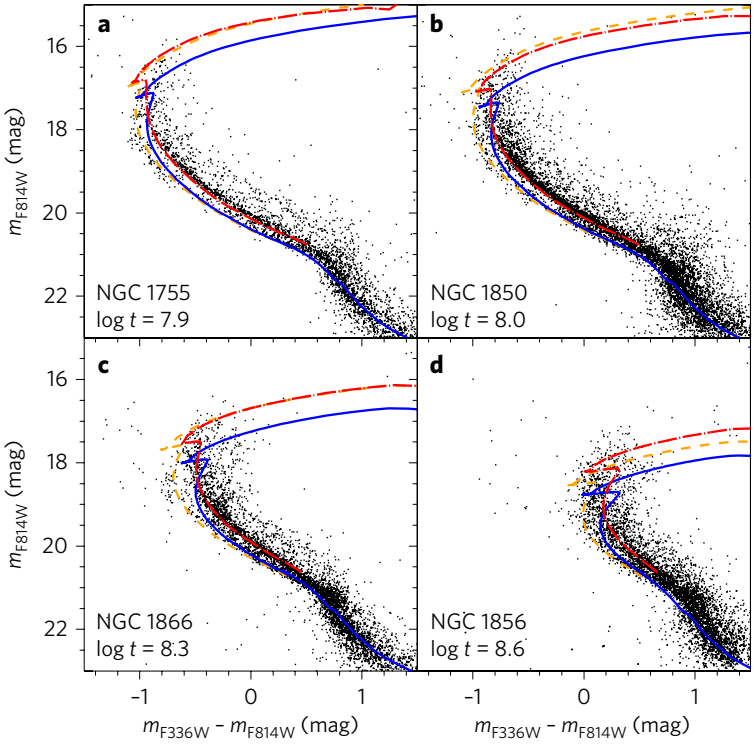

Figure 1.2.7: CMD of four YCs, taken from [D'Antona et al., 2017]. Red isochrones are fast rotating isochrones ($\omega = 0.9\omega_{crit}$) while blue ones are coeval (with respect to red isochrones) non rotating one. Orange isochrones are non rotating isochrones younger by 0.1 dex the the ages at the bottom, fitting the upper part of the TO region.

star reaches its final location on the CMD. Only if this takes place before the end of the MS the star shifts on the bMS. On the other hand, if the braking process ends after the end of the MS, then the star evolves directly from the rotating MS (rMS), thus populating the upper part of the MSTO.
So, a star moving from the rotating (rMS) to the non-rotating track, at fixed X_c, will appear younger as soon as braked, but its MS lifetime will be shorter, thus simulating an older isochrone. This mechanisms then accounts for both the presence of younger stars on the upper bMS, and of older stars in the TO region.
The brighter part of the bMS host stars which have been braked less then 25% of the cluster age ago, since they haven't already left the MS.
In conclusion, rotational evolution, produces different timescales for the core hydrogen-burning phase which can be perceived as a mixture of stellar ages, with stars on the bMS being completely braked, and dimmer TO stars being stars whose envelope is not completely braked. The younger population (in orange in Figure 1.2.7) is then composed of recently braked coeval stars, thus mimicking a younger stellar generation.

1.2.5 Summary

We summarize here the properties of the observed CMDs of these cluster, in order to compare predictions of the two models with these requirements.
As said before, no study found evidence for chemical abundances variations in IACs and YCs star, questioning the analogy between these clusters and old GGCs. Then, [Goudfrooij et al., 2014] found a correlation between cluster mass and age variation which

Properties	**Age spread**	**Rotation**
No chemical abundances variations between stars	✗	✓
Presence of an eMSTO if age < 2 Gyr	✓	✓
Presence of a split MS if age < 1 Gyr	✓	✓
Relation between pseudo-age spread with cluster mass	✓	✗
Relation between pseudo-age spread with cluster age	**ad hoc**	✓

Table 1.1: Observed properties of multiple populations in Magellanic Clouds clusters compared with the predictions of the *age spread* model and the *rotational* one.

is expected from the age-spread scenario, but it is completely inconsistent with the rotation scenario. Finally, [Niederhofer et al., 2015] and [Goudfrooij et al., 2017] found a relation between pseudo-age spread and cluster age, in the sense that the width of the TO increases with cluster age. The dataset is however composed mostly of intermediate-age clusters. In table 1.1 we summarize observed properties, checking whether they are reproduced or not by the two models. The checkmark does not mean that the requirement is fulfilled, but only that it could be in agreement with the scenario.

1.3 Thesis layout

In this work I will determine the age distribution of TO stars for nearly 27 Magellanic Cloud clusters with age between 40 Myr and ~ 2.5 Gyr in order to find the age spread of Turn-Off stars. The goal is to use the relations between cluster age, age-spread and possibly mass to determine the nature of this spread. I will compute the theoretical relation between age and age spread according to the rotational scenario using `SYCLIST` models for rotating stars, and finally I will compare the results with theoretical predictions. Additional analysis will be explained in next sections.
Together with this analysis I will derive high-precision photometry for two peculiar clusters, which have never been investigated in the context of multiple populations.

The layout of the thesis is as follows: In the Chapter 2 I present the data and the data reduction. The data analysis is described in the Chapter 3, while results are presented in the Chapter 4 where I also provide some discussion and conclusion.

CHAPTER 2

Data Reduction

To investigate the multiple-population phenomenon in Magellanic Cloud star clusters I used high-precision HST photometry of 27 young and intermediate-age clusters of both the LMC (20 GCs) and the SMC (/ GCs). For the majority of clusters I used the astrometric and photometric catalogs derived as a part of the HST survey of multiple populations in Magellanic Cloud star clusters [Milone et al., 2009] and series of papers and references there in).
The literature catalogs include astrometry and multi-bands photometry of 25 clusters with ages between $\sim 40 \quad Myr$ and $\sim 2.5 \quad Gyr$. Table 3.1 summarizes the main properties of these clusters.
The data of two clusters, namely KMHK250 (RA(J2000); DEC(J2000) = 04 54 29.0; −69 55 12) and NGC265 (RA(J2000); DEC(J2000) = 00 47 11.4 ; −73 28 37), have been reduced and analyzed for the first time in this work. Both clusters were not included in the survey and never investigated in the context of multiple populations.
In this chapter I will describe the dataset and the procedure that I used to reduce the images of KMHK250 and NGC265, which is similar to the procedure used to derive photometric and astrometric catalogs from the HST survey of multiple populations in Magellanic Cloud star clusters. I refer to the series of papers by [Milone et al., 2009] and references therein for details on the reduction of the images of the remaining clusters.

2.1 Instrumentation

To investigate the effects of age and rotation in the CMDs of Magellanic Cloud clusters I need high-precision photometry of relatively-faint stars at the distance of the LMC and the SMC. The Hubble Space Telescope (HST) is the only telescope that makes it possible to derive accurate measurements of fluxes and positions in the crowded environments of extragalactic globular clusters.
Indeed HST, which is a geostationary orbital telescope working since 1990, played a fundamental role in recent astronomy discovery, and among its outstanding achievements, the discovery of multiple populations in several Galactic and extragalactic globular clusters is one of the most intriguing.
Being outside earth atmosphere, HST is sensible to wavelengths that would be inaccessible from Earth observations, like for example the UV band $(\lambda = 10 - 400)nm$. The ultraviolet spectral region is crucial to identify and characterize multiple populations with different helium and light elements abundance in old clusters, and stellar populations with different rotation rates in young clusters.

HST currently host 6 different instruments on board:

- Advance Camera for Survey (ACS)
  - Wide Field Camera (WFC) : WFC is the Wide Field Channel of the Advanced Camera Survey: $\lambda = (3500 - 11000)$Å
  - High Resolution Camera (HRC)
  - Solar Blind Camera (SBC)
- Cosmic Origins Spectrograph (COS)
- Wide Field Camera 3 (WFC3)
  - UVIS: $\lambda = (2000 - 11000)$Å
  - IR
- Near Infrared Camera and Multi Object Spectrometer (NICMOS)
- Space Telescope Imaging Spectrograph (STIS)
- The Fine Guidance Sensors (FGS)

The data of KMHK250 and NGC265 are collected through the *F435W*, *F555W* and *F814W* filters of ACS/WFC, while the data of the other clusters reduced by [Milone et al., 2009] and series, come from both ACS/WFC and WFC3/UVIS. We add here that the optimal filters combination to detect multiple populations in young cluster is the WFC3/UVIS *F336W* and *F814W*, and most of my analysis uses the *F336W-F814W* vs. *F814W* Color Magnitude Diagram.

2.2 Data Reduction

Stellar astrometry and photometry for newly reduced clusters have been carried out by analyzing bias and flat-field corrected images, using the procedure and the computer programs developed by Jay Anderson [Anderson et al., 2008] and reference therein. The images have been first corrected for the effect of the poor charge transfer efficiency (CTE) following [Anderson and Bedin, 2010] by using the software written and provided by these authors. Briefly, they have developed a model that reproduces the trails observed in a large sample of analyzed dark exposures. Their software converts the observed into an estimate of the original pixel values by inverting the derived model.
Every step discussed in the following section has been done both on the cluster KMHK250 in the LMC and NGC265 in the SMC. For both clusters we downloaded images from HST MAST in *F435W*, *F555W* and *F814W* ACS/WFC filters.
The data reduction is based on Point-Spread Function (PSF) photometry. I will now explain in detail the procedure with which the fortran routines compute the PSF for every image.

2.2.1 Effective PSF

In order to derive astrometry and photometry of multiple point sources, we need only three parameters, which are the position of the source (x, y) and its flux (f). These parameters are derived from the array of pixels that constitute the image of the star, and by using the Point-Spread Function.
The PSF in Charge Coupled Devices (CCD) is given by the convolution of two functions that unfortunately we do not observe directly. The first one is the instrumental PSF (iPSF) which gives the flux for a point source as a function of offset from its center, and the second one is the pixel response function that gives the sensitivity at each point in

the pixel. In order to derive a reliable PSF model we should, in principle, know these two functions.
[Anderson and King, 2000] developed an innovative approach, which is based on the Effective PSF (ePSF) and is able to bypass the need to know the two functions. The ePSF consists in a continuous function of $(\Delta x, \Delta y)$, offset from the center of the PSF, whose value at any point is the fraction of light of a point source that would fall in a pixel centered at that point. Then, instead of forcing this function into a purely analytical function, it is treated in an empirical way and its value is tabulated at an array of points. Since HST is an orbital telescope its observations are not affected by seeing, which, for Earth observations, tends to distribute the PSF on more pixels, so that the Full Width at Half Maximum (FWHM)of the iPSF is generally 2-3 pixel. However, in HST ACS/WFC images, the typical PSF has a core of about 50 *mas*, which is, moreover the pixel size (50 *mas* for ACS/WFC channel). This effect goes by the name of "undersampling" and leads to some problem in deriving the correct PSF since most of the flux of the star falls into the central pixels. This leads in turn to a degeneration in the PSF, and a "pixel-phase error". We show this effect in Figure (2.2.1), where we cannot distinguish between the two PSF model since they are both correct. To avoid such problem the "dithering" technique is used. It consists of taking images slightly shifted, so that stars move from one image to another, breaking the degeneracy in the PSF model.

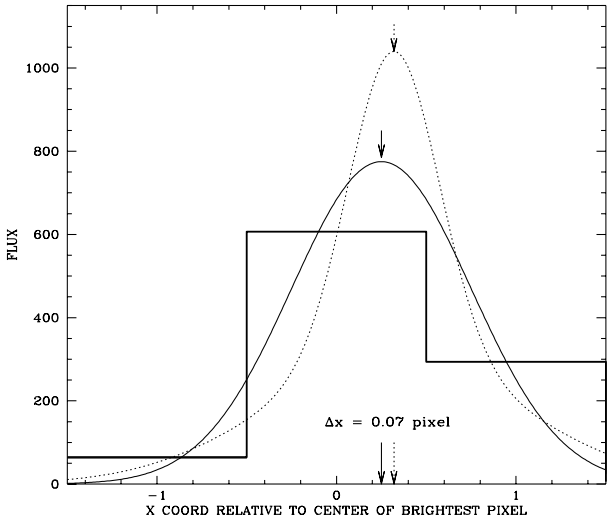

Figure 2.2.1: One-dimensional star profile, with two different PSF models superimposed. Both models fit the pixels value correctly, but the location of their peaks is slightly different. Figure from [Anderson and King, 2000]

Another issue is that, because of position-dependent charge diffusion and optical aberrations, the PSF may change shape with location on the detector. In order to derive the best possible PSF, which translates in the best possible photometry and astrometry, the fortran routines I used in this work account for spatial variations across the field of view. In order to account for spatial variability, instead of a single PSF the program computes a grid of 9×10 fiducial PSFs, as in figure 2.2.2. Then a PSF is built for any point in the detector simply interpolating the PSF among the four nearest grid points. In addition to spatial variability, PSF core changes over time with the change of focus, and this effect is called "breathing". Since this time variability is decoupled from the spatial variability, we can represent the PSF as a sum of a library PSF and a small perturbation PSF, built from the residuals of the fit of the star flux with the library PSF.

In the following section I will explain how astro-photometric catalogs have been derived. In particular HST images can be reduced in two different ways, I will refer to these as

"method 1" and "method 2".

- **Method 1:** first every image is reduced singularly, and then the information from every image in the same filter is put together, as described below
- **Method 2:** every image in the same filter is stacked in a single image, and then positions and magnitudes are computed from every stacked images.

The difference of the two methods is mainly the precision acquired for faint and bright stars. Method 2 in fact improves the quality of the measurement of faint stars, because the stacking process increases the low Signal-to-Noise ratio (S/N) of these stars, but, on the other hand worsen the accuracy for bright stars. Method 1 instead works the other way round, increasing the precision for bright stars. In this work I am interested in TO stars, which are bright stars, so method 1 is the one that would give better results. However, in order to release clusters catalogs in the future, I used also method 2 to derive the photometry of faint stars, which will be then used to create the final catalog.

2.2.2 Catalog Building

To derive the PSFs grids that best reproduce the observed stellar profiles of each image, I used the fortran routine `img2psf` [Anderson and King, 2000]. This routine exploits the information from all the isolated, bright, and non-saturated stars of each exposure to derive an extremely-accurate ePSF by using the method described in the previous subsection. Basically it uses a pre-computed library PSF, according to the filter in which the image is taken, and uses this PSF as a starting guess to derive the grid of PSFs discussed before. To compute the best possible PSF the routine takes at least 7 arguments:

- **Isolation index** is used to select isolated stars. It specifies how far away from a brighter pixel a peak in the image must be in order to be used to compute the PSF;
- **Minimum flux** for a source to be considered in the determination of the PSF model. Since we are interested in bright stars only, I used FMIN=3000;
- **Maximum flux** for a source to be considered in the determination of the PSF model. It allows to exclude saturated stars. Since saturation in HST images starts at 55000 DNs, I used PMAX=54999;
- **Maximum Q-fit** of a star fitted with the library PSF in order to be used to determine the PSF grid. The Q-fit is a parameter indicative of the quality of the fit. By setting QMAX=0.2 I excluded nearly all the non-stellar sources, like galaxies and cosmic rays and blended stars;
- **Number of regions** in which I divided the image to find the perturbation PSFs. It ranges from 1 to 5. The adopted value of NSIDES is the result of a compromise. Indeed, on one side, I would need a large number of regions to account for small-scale non-linear variations of the PSF across the chip. On the other hand, a small value of NSIDES would maximize the number of stars used in the PSF determination. I fixed a value of NSIDES=3 on the basis of the stellar density of each image. I verified that a larger value would result in a poor PSF model, due to small number of stars in each sub-region;
- **Initial PSF guess**. Library PSF for the initial fit;
- **IMG.fits**. Image to analyze.

After deriving the PSF, I used `img2xym`, a fortran routine by Jay Anderson to determine positions and fluxes of stars in the image by fitting the best-model PSFs to the stars of each image (see [Anderson and King, 2006] for details).
Similarly to the routine `img2psf`, this program takes as input parameters again the isolation index, the minimum and the maximum stellar fluxes. In contrast with what I

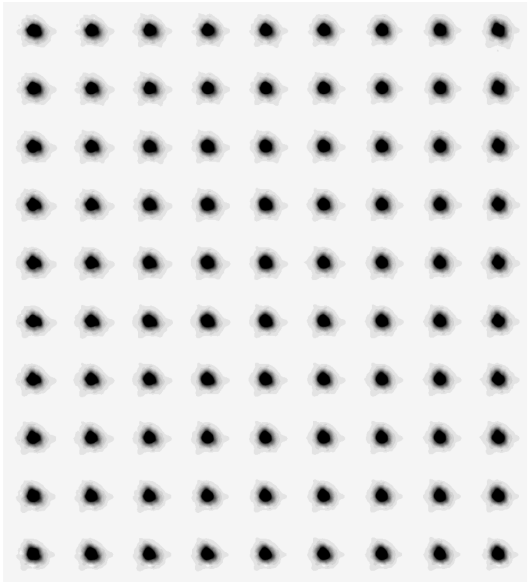

Figure 2.2.2: Example of the 9×10 grid of fiducial ePSFs

have done in the previous program, in this case I would need every stars to be analyzed and fitted with the PSF, including the saturated ones. As an additional check I used the SUBT flag, which tells the program to generate a subtracted image after measuring all the stars in each image.
The program generates then a `txt` file with extension `xym`, which has 4 columns, namely `x y mag q-fit`, where `x` and `y` are the coordinates of the stars in the reference frame of the image, `mag` is the stellar magnitude in instrumental units and is defined as

$$mag = -2.5 \log(flux)$$

where the flux is expressed in photo-electrons recorded in the reference exposure, and the `q-fit` is indicative of the quality of the fit between the observed star and the best-model PSF. Thanks to the quality fit parameter we can now discriminate between stars and other sources. A perfect fit would have in fact a `q-fit` equal to 0, and the greater its value is and the worse the fit is.
To discriminate between the effects of age and rotation in the cluster CMD, I would need high-precision photometry. For this reason, I analyzed only those stars with relatively-small values of the q-fit parameter. I developed a SuperMongo macro, which selects only the best-measured stars by using the following procedure.
I began dividing all the stars into magnitude bins, with the size of each bin varying from one cluster to another and from one image to another depending on the number of stars; for each of them, I computed the median q-fit and the 68.27th percentile (hereafter σ). The median was derived recursively: after each computation, all stars exceeding four times σ were provisionally rejected until the next iteration and the median was recomputed. This procedure was repeated until two subsequent measures of the median differ by less than the 1%. Finally, I added to the median of each bin N times σ and linearly interpolated these median points to derive the blue line shown in Figure 2.2.3. All stars below this line in each plot were flagged as well-measured. The factor N ranges from 5 to 6, and was chosen to draw the boundaries that follow the bulk of the distribution of each parameter value. The result of the selection is shown in Figure 2.2.3, where small red dots are the selected stars. Note that, although the qfit is far from 0, I did not eliminate saturated stars ($m_{F814W} < -13.75$) because they will be used in the next step.
After repeating the procedure for every image in the same filter, I am left with one catalog for every image containing positions and magnitudes. Since images are different,

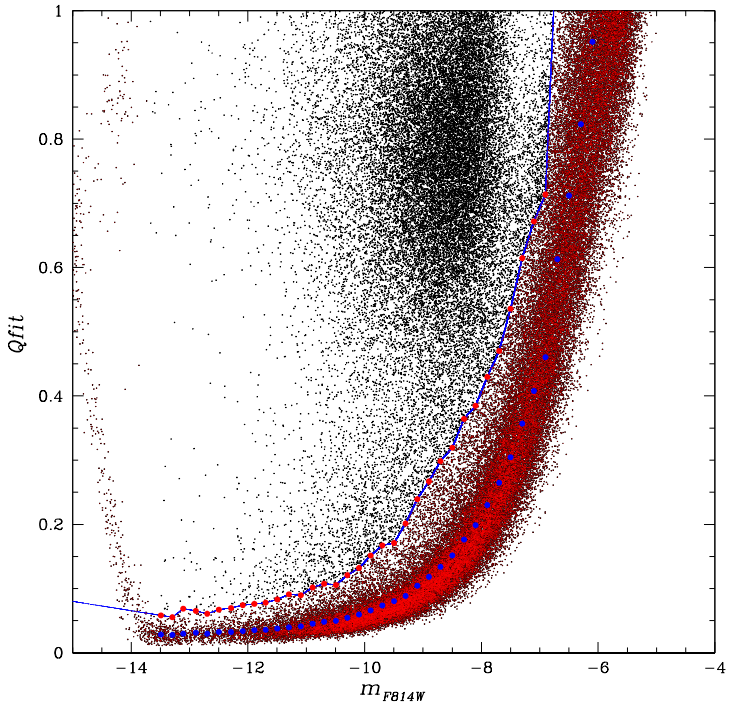

Figure 2.2.3: Qfit clipping results for the image `90601acq_WJC` of NGC265. Stars in red are the ones that will be used in further procedure, while black dots are poor fitted objects, and thus they are not included in the analysis. Blue and red bigger dots are the median value of every bin and the median plus 3σ.

each catalog will have its own reference frame, and in order to proceed I need to find the right coordinate transformation from one to another, creating thus a single reference catalog.
In order to do this I used again a set of fortran routines by Jay Anderson: `xym2mat`, `xym2bar` and `xym1mat`. The first program finds the parameter of the linear transformation between a set of input catalogs and a reference one, and corrects them for geometrical distortion, according to the selected filter and chip. `xym2bar` generates one single catalog for every filter in which the magnitude of a star is computed as the mean magnitude. In order to account for the exposure time I slightly modified this part, weighing the final mean magnitude with the exposure time. This leads to a better estimate of the magnitude, since it does not mix long exposure images with short ones.
Finally `xym1mat` links two catalogs in different filters, creating a final astro-photometric catalog with magnitudes in the given filters combination.

Cross Identification

To find the correct transformation between catalogs these programs use a method called *Cross identifications*. This is based on the fact that triangles do not change their basic shape (they remain similar) with translation, rotation, scale change or flip. Then, each triangle contains two independent and invariant shape parameters that can be used to classify and recognize its :

- **b/a**. ratio of the triangle's intermediate side (b) to its longest side (a)
- **c/a**. ratio of the triangle's shortest side (c) to its longest side (a)

Thus, given some triangle defined by three points in the CCD space $(x, y)[PIX]$, it can be identified by a point in two-dimensional space $(b/a, c/a)$, and the same three stars will always be represented by the same point in this space, independently from the transformations they suffer.
First the program identifies common stars in the catalogs and then derives the parameters of the transformation. The number of parameters depends on the transformation itself, and there can be upto six parameters in the case of rotation, translation, tilt and scale change, so that the general formula is

$$\begin{cases} x_1 = A + C \cdot x_2 + E \cdot y_2 \\ y_1 = B + D \cdot x_2 + F \cdot y_2 \end{cases} \tag{2.1}$$

Using then these transformations the software converts positions and magnitudes of stars into the chosen reference system, selecting only stars present in at least a minimum number (`NIMMIN`) of catalogs, its value being user-selected. Finally, the program generates some, MAT.xxx files, one for each catalog given in input, containing positions and magnitudes in the reference catalog, the transformed values and the residuals of the transformations. If the program worked correctly residuals should have, moreover, a spherical distribution centered at 0, like in Figure (2.2.4).

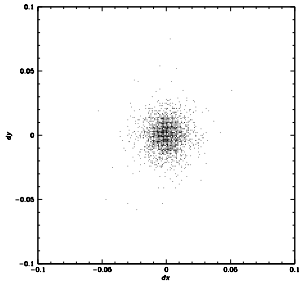

Figure 2.2.4: Residuals of the transformation

Final Catalog

Using the program `xym2bar` I the created one final catalog, with mean positions and magnitudes of the single catalogs. I repeated this procedure for every filter, so that, in the end, I would have one single file for every filter, with positions and magnitudes for every measured stars. At this point, `xym1mat` finds common stars given two input catalogs, and writes a file with positions and magnitudes of these stars. Here I used this program with catalogs in different photometric bands, in order to have mean positions and mean magnitudes in different filters. To speed up the process, I first linked just bright stars in order to find the transformations, and only then I made the program link all the stars.
The next step would be that of creating the CMD in some chosen filters. However, while the procedure now described works well with bright stars, it does not provide the same degree of accuracy for faint stars, since their flux is quite low. To analyze faint stars it would be much better to sum the flux of a star in different image (in the same filter), increasing Signal-to-Noise ratio (S/N), and thus the photometry precision.

Gaia Fixing

I want these catalogs to be as precise as possible, both in positions and magnitudes. So, in order to achieve the best possible accuracy, I linked these catalogs with a GAIA one, downloaded from `https://gea.esac.esa.int/archive/` for the specific cluster field. Using `xym1mat` I linked the GAIA catalog with a previously create HST one, creating a

catalog with x, y from the Gaia catalog and magnitude from the HST one. I refer to this catalog (one for every filter) as the "Master Frame". Finally, I used these as reference frame for `xym2mat`. I iterated different times in order to have the highest precision, getting in the end the final catalog for each filter.

Stacked Images

To accomplish the faint stars analysis, I used another fortran routine by [Anderson et al., 2008], `KS2.F`. This program is, by bar, the most complex among the ones I used in this work. First of all it computes astrometry and photometry both in individual images (method 1) and in stacked images (method 2), giving in output both catalogs. As said before, in method 2, the program stacks all the images in a given filter, or better, in a given group specified by the user. I separated in fact long exposure images from short exposure images, even if taken with the same filter, in order not to compromise the quality of the analysis. We can see the different results of the two methods in Figure (2.2.5), where in panel (a) photometry has been computed with method 1, and we have a larger dispersion for faint stars ($m > -8$) while in panel (b) method 2 provides a much better photometry for faint stars, but increases the spread in color for bright stars. In this dataset the difference is not as noticeable as one would think. The reason is that on HST archive only 2/3 image per filters of KMHK250 were available, and so the stacking process increases the S/N just slightly.
As additional output `KS2` returns one stacked image for every specified group, in which every pixel value is the number of image in which that particular pixel has been measured. This image is quite useful since it tells us which was the field of view of every image.

Using the stacked images I then created a RGB image of the field (Figure 2.2.6).
Finally, the program gives the user the possibility of measuring artificial stars (AS). It takes as input a list of stars with given position and magnitude, and analyzes them as if they were real stars. From the comparison between the real values (input) and the measured ones (output) we can estimate photometric errors, which, though not 100 % correct, is by far the best we have.
At this point, I need to calibrate magnitudes, in order to have scientific results comparable with the literature.

2.3 Calibration

In order to calibrate the magnitudes, I compared the instrumental magnitudes computed as PSF photometry, with magnitudes computed as aperture photometry on `drz` images. First of all some informations about drz images, since these images are quite different from the ones analyzed so far. They are in fact a sort of stacked images, with exposure time normalized to one, so that the pixel values are actually the number of photons per second.
Calibrated magnitudes are computed as

$$m_{cal} = m_{inst} + \Delta mag + ZP_{filt} + C \tag{2.2}$$

where Δmag is the difference between PSF magnitude and AP magnitude computed as explained below, ZP is the zero point correction for a given filter, and C is the aperture correction, which accounts for the totality of the flux, considering the aperture used. The latter two have been downloaded from `http://www.stsci.edu/hst/acs/analysis/zeropoints`, considering the date of the observation, the filter used and the selected aperture radius.
With aperture photometry I can, in principle, use all the flux of a star, simply increasing the aperture radius. The problem is that increasing the radius too much, I would get

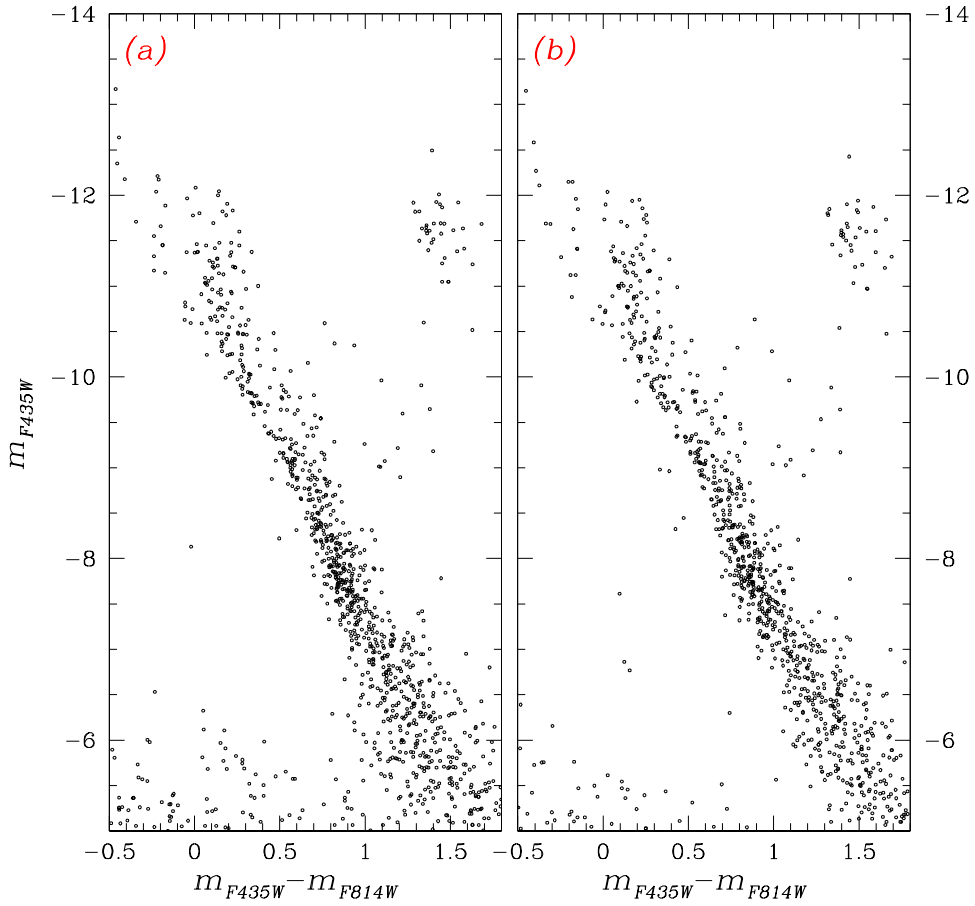

Figure 2.2.5: Panel a): photometry determined on single images, method 1. Panel b): photometry derived from stacked images, method 2. We can see that faint stars are much narrower in method 2 than method 1, while, on the other hand method 1 increases the quality of the photometry of bright stars. The final catalog will use faint stars measured with method 2, and bright stars with method 1.

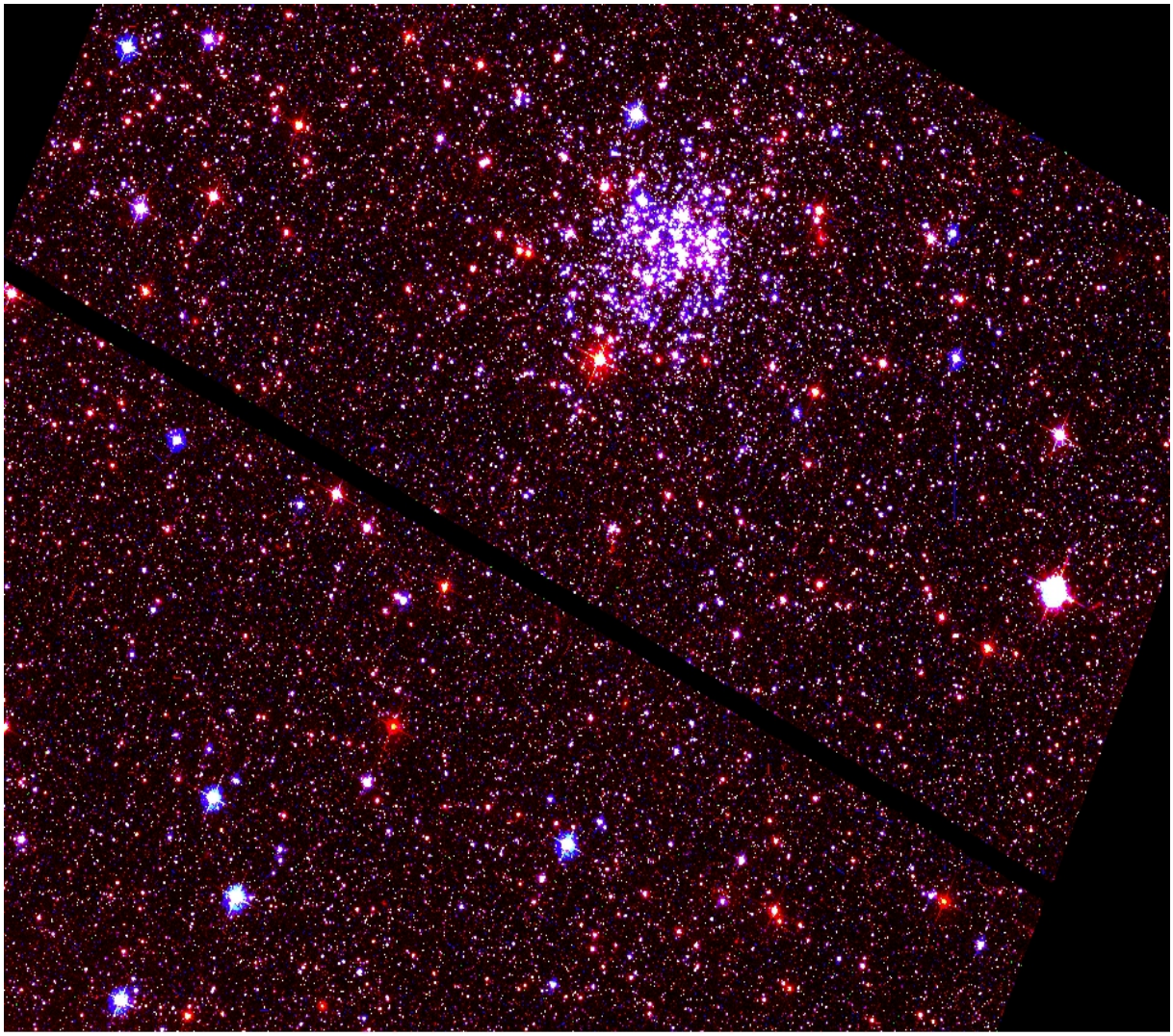

Figure 2.2.6: Trichromatic stacked image of NGC265

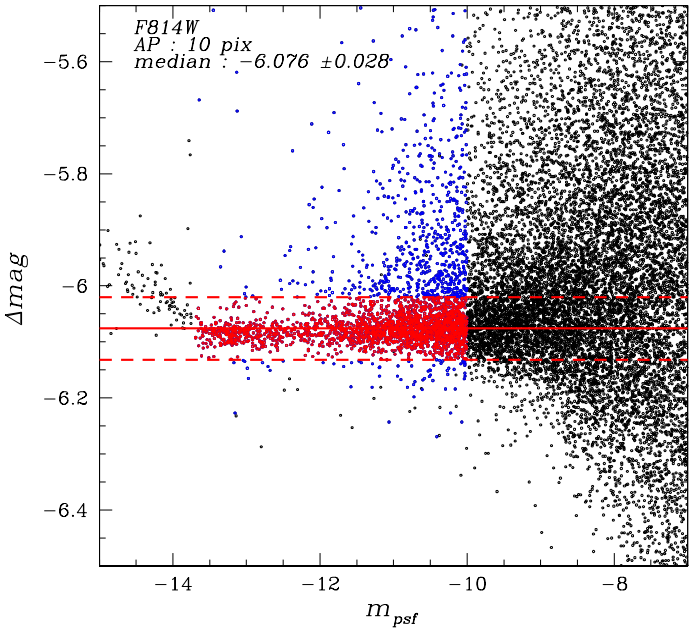

Figure 2.3.1: Clipping procedure for determining Δmag for a given aperture. Red and blue stars represent the first selection, in which we choose only bright stars. I compute then the median value, and select stars with Δmag between 2σ (dashed red line) from this value (only red stars), and we recompute the final median value (solid red line).

not only the flux of the star I am measuring centering the aperture on, but also that of other stars, which I do not want. The idea is then to increase as much as possible the radius, without including other source's flux. To determine the ideal radius, I first used another Jay Anderson fortran routine `drz_phot_gfortran.F`, which computes aperture photometry, given the aperture radius (in pixel) and the inner and outer sky radius, and then I wrote an apposite macro in SuperMongo to determine the median Δmag_{AP}^{PSF} for every aperture and its dispersion. This macro then is called for a set of aperture radii. The first step, after the computation of the aperture photometry on a given image, is to link the new catalog to the PSF photometry one, in order to have, for every stars, both PSF and AP magnitude.

Then, the macro in SuperMongo computes the difference between PSF magnitude, and AP magnitude of bright stars, and for every aperture finds the median value with its error. Finally it builds the "growing curve", which shows the difference in magnitude between the two photometry approaches, versus the aperture radius in pixel. The result is a curve that saturates after some radius value, with the error on the median value increasing itself. Figure (2.3.1) shows how the median value is computed. First of all I only want to use bright but not saturated stars, for example in range $-13.75 < m_{PSF} < -10$ because they are better measured, then I compute the median value of this sub-dataset, and its sigma. Finally I re-compute the median value clipping between 2σ from the previous median value, and I get the final Δmag with its dispersion. We repeat the procedure for every aperture, finding the the curve in Figure 2.3.2. As we can see, after $10pix$ the value of Δmag becomes almost constant, but the error does not, and that tells us that $10pix$ is the optimal aperture radius to use as input for the program.

The aperture correction is then downloaded for this specific value of the aperture, considering that ACS/WFC has a pixel scale of $0.05pix/arcsec$. This is the last step of the calibration process, and once done that I can create a high precision astro-photometric catalog with calibrated magnitudes. At this point I proceeded with the data analysis,

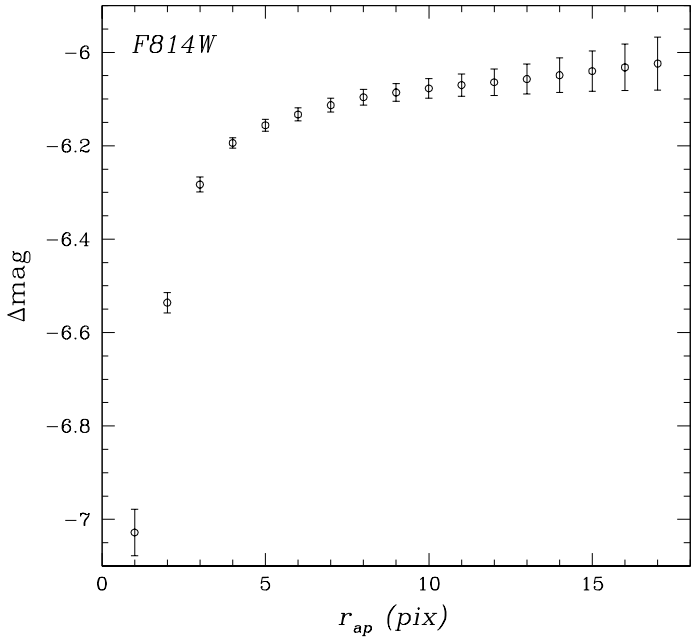

Figure 2.3.2: Δmag vs. aperture radius in pixel. It is clear that the dispersion of Δmag increases with the radius, as well as Δmag itself. However, for an aperture greater than $\sim$ 10 pixel, its value is almost constant while the dispersion keep increasing, as expected because are no longer measuring just the flux of the source, but also external contamination.

determining the age distribution of TO stars in every cluster.

CHAPTER 3

Data Analysis

This chapter describes the procedure I developed to determine the age distribution of turn-off stars in young and intermediate-age clusters in Magellanic Clouds. Since I am interested only in cluster stars, it is essential to remove field stars from our analysis. Therefore the first step of the procedure has been that of correcting the data for field contamination, statistically subtracting field stars, as explained below.
First I will present the dataset used in this work, and then I will give details on the procedure used to compute the age distribution of TO stars.

3.1 Dataset

In this work I used the first large sample of young and intermediate-age clusters in Magellanic Clouds (collected GO-14710 PI. A. P. Milone, GO 13379, GO 14204) combined with HST archive multi-band images of intermediate-age clusters. The images were obtained through the Ultraviolet and Visual channel of the Wide-Field Camera(UVIS/WFC3), and ACS/WFC, both on board of HST. I used images in the *F336W*, *F438W* and *F814W* bands in UVIS filters, and *F435W*, *F814W* in ACS filters. The final dataset counts 27 clusters, both in the LMC and the SMC, with an age in the range ($40Myr$-$2.8Gyr$). The first part of this thesis has been that of learning and mastering the data reduction process described in chapter 2, applying the procedure on two particular clusters. Then, I developed a technique to determine the age distribution of turn-off stars in a given cluster, to correctly interpreting the results in the context of the scenarios described in Chapter 1.
In Table 3.1 is shown the complete dataset with the cluster's main properties.

3.2 Sample Correction

Before proceeding with turn-off stars analysis I determined the cluster radius on the image and then I statistically subtracted field stars. The cluster radius has been derived by eye with the criteria of selecting a region that is mostly populated by cluster members without including too many field stars (red circle in Figure (3.4.1). In the following we will refer to this region as "cluster field".
In the particular case of the cluster KMHK250, which is an extremely loose cluster, I determined the radius with a more rigorous procedure, first computing the density distribution, and then taking the value for which the density became nearly constant.
Every cluster has been then corrected for field contamination and differential reddening,

Cluster	galaxy	RA (J2000)	DEC (J2000)	$\log(\mathcal{M}/\mathcal{M}_\odot)$
KRON 34	SMC	00 55 33.50	−72 49 56.00	—-
NGC 152	SMC	00 32 56.26	−73 06 56.60	—-
NGC 294	SMC	00 53 04.94	−73 22 45.70	4.40
NGC 265	SMC	00 47 11.40	−73 28 37.00	—-
NGC 330	SMC	00 56 18.59	−72 27 48.10	4.61
NGC 411	SMC	01 07 55.95	−71 46 04.50	4.67
NGC 419	SMC	01 08 17.79	−72 53 02.80	5.38
NGC 1651	LMC	04 37 32.53	−70 35 08.71	4.91
NGC 1755	LMC	04 55 15.53	−68 12 16.80	3.60
NGC 1783	LMC	04 59 08.59	−65 59 15.84	5.42
NGC 1801	LMC	05 00 34.57	−69 36 46.20	4.26
NGC 1805	LMC	05 02 21.73	−66 06 42.60	3.70
NGC 1806	LMC	05 02 11.00	−67 59 18.00	5.10
NGC 1818	LMC	05 04 13.42	−66 26 03.10	4.41
NGC 1831	LMC	05 06 17.40	−64 55 11.00	—-
NGC 1846	LMC	05 07 34.90	−67 27 32.45	5.24
NGC 1850	LMC	05 08 45.20	−68 45 38.70	5.04
NGC 1852	LMC	05 09 23.76	−67 46 38.00	4.66
NGC 1856	LMC	05 09 30.21	−69 07 44.40	5.07
NGC 1866	LMC	05 13 38.77	−65 27 51.40	4.91
NGC 1868	LMC	05 14 35.80	−63 57 14.00	4.34
NGC 1953	LMC	05 25 28.07	−68 50 16.50	4.20
NGC 1978	LMC	05 28 45.33	−66 14 12.04	—-
NGC 1987	LMC	05 27 16.94	−70 44 14.16	4.74
NGC 2164	LMC	05 58 55.89	−68 30 57.50	4.18
NGC 2173	LMC	05 57 58.00	−72 58 42.00	4.67
KMHK 250	LMC	04 54 29.00	−69 55 12.00	—-

Table 3.1: Properties of the analyzed clusters. Cluster masses are taken from [Milone et al., 2018] and [Goudfrooij et al., 2014].

when needed. Given the large number of clusters analyzed I will show this procedure for one single cluster, NGC 419, while for others I will recall only the results.

3.2.1 Differential Reddening

A significant spatial variation of the reddening across the field of view results in a broadening of stellar colors the magnitudes in the CMD, given to the different degree of absorption of light across the field of view. Thus, as we aim to estimate the color broadening in the TO region, we may need to correct our photometry for the effect of differential reddening in order to properly investigate turn-off stars.
The differential reddening suffered by each star has been determined in [Milone et al., 2018], and the only two clusters whose photometry is significantly affected are NGC 1850 and NGC 1856. We show in Figure (3.2.1) the results of the correction for the cluster NGC ,1856 within its central region.

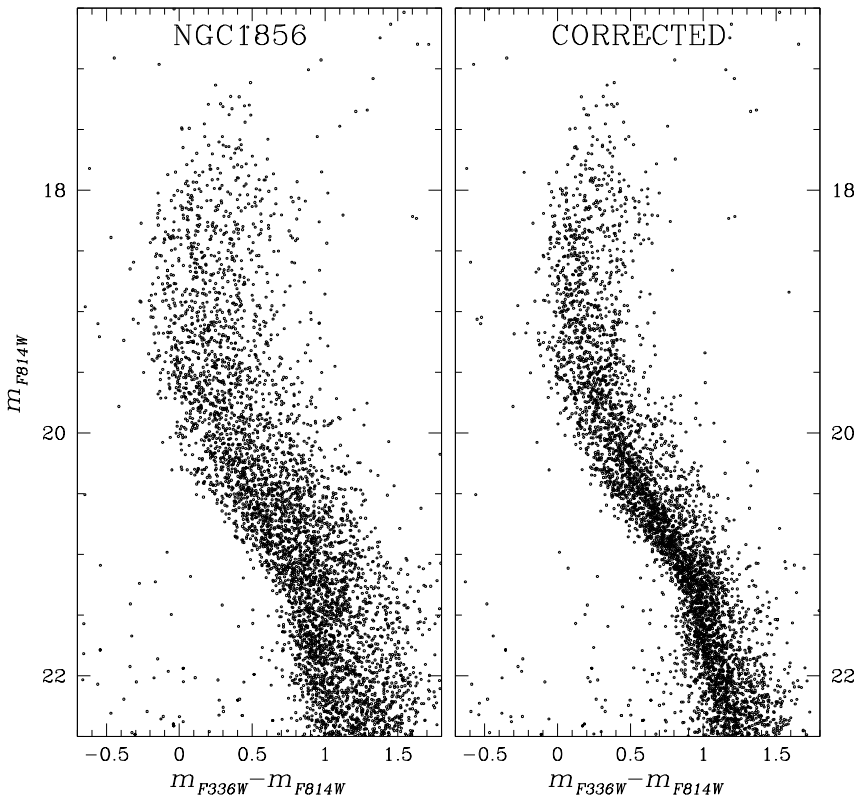

Figure 3.2.1: Differential reddening correction for NGC ,1856. The left panel is the CMD as observed, while the right panel is the corrected CMD.

As we can see the spread in color in the left panel (not corrected for differential reddening) is much larger than that in the right one, and without the correction, the results of our TO stars analysis would be wrong.

3.2.2 Statistical Subtraction

Decontamination from field stars has been carried out using a statistical method which is based on the comparison between the cluster field and the reference field. After selecting

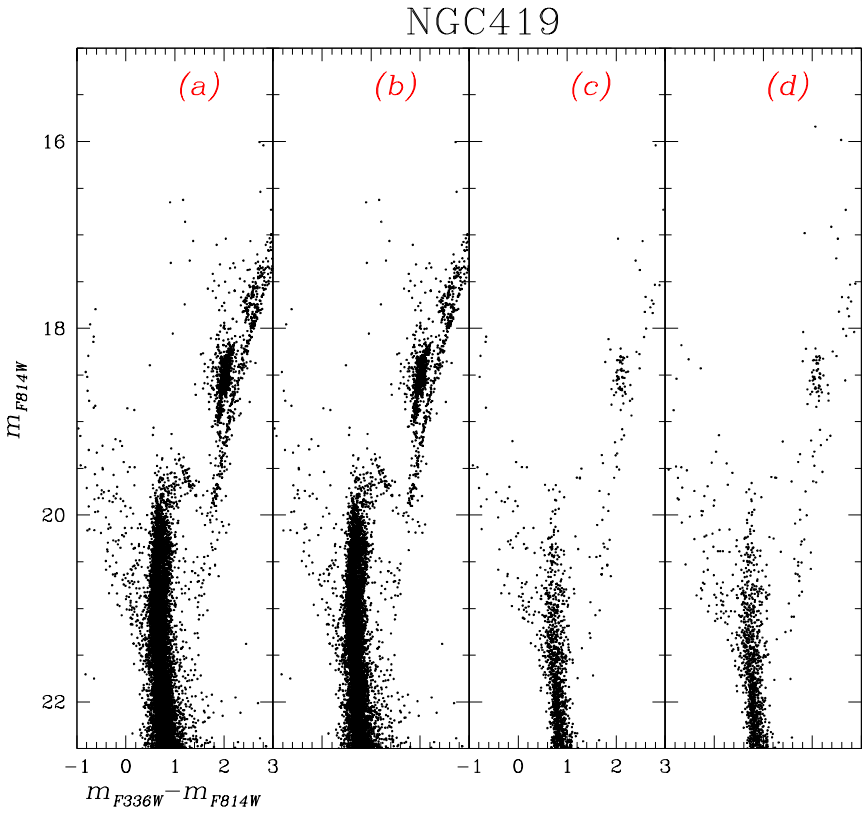

Figure 3.2.2: Statistical subtraction for cluster NGC419 in the LMC. Panel (a) shows CMD for stars in cluster field and panel (b) the decontaminated cluster field CMD. Panels (c) and (d) shows stars subtracted from the cluster field and stars selected according the value of the random number criteria from the reference field.

the cluster field, as explained above, the reference field has been identified as a region including only field stars (blue circle in Figure (3.4.1)).
In order to statistically subtract the stars of the reference field from the cluster field CMD I have used the procedure described in [Milone et al., 2009] and series. This method is based on the association between each star in the reference field with a star in the cluster field, which has the closest position on the color-magnitude plane. Since the areas of the two regions are different, the reference area $A_{\rm field}$ field being much larger than the cluster one $A_{\rm cluster}$, in order not to over-subtract I generated random number k_i in the range $(0, 1)$ for each reference field star, and I subtracted just the ones for which $k_i < \frac{A_{cluster}}{A_{field}}$. Then, for each of these stars I computed the distance d_i from every cluster field star in the color-magnitude plane and subtracted the nearest star from the cluster field.

$$d_i = \sqrt{(col_{cl} - col_{ref,i})^2 + (mag_{cl} - mag_{ref,i})^2} \tag{3.1}$$

In order to subtract only stars representative of the reference field CMD, the maximum distance for the star to be subtracted has been set to $d_i = 0.05$. We can see the result of the procedure in Figure 3.2.2. Panel (a) shows the complete CMD, and panel (b) is the decontaminated CMD. Panel (c) and (d) are respectively the CMD with stars subtracted from the cluster field and selected stars from the reference field. As expected the CMDs in panel (c) and panel (d) are almost identical, meaning that the procedure has succeeded.

3.3 Pseudo-age Distribution

Once obtained clean data, without field contamination nor differential reddening I determined the age distribution of TO cluster stars.
First of all I assumed that the spread in the Turn-Off region is given by star-to-star age variation, as predicted by the "age-spread" scenario. Therefore, a consequence of this assumption is that every star in the CMD has its own age, which is determined by the best fit isochrone. Stars in the Turn-Off region are then interpolated with a dense grid of non rotating isochrones with different ages, taken from [Marigo et al., 2017] using the web-tool http://stev.oapd.inaf.it/cgi-bin/cmd_3.0.
In the following I describe the different steps of the procedure to derive the pseudo-age distribution:

I *Turn-Off region.* First, I defined the TO region, which has been selected as a rectangle with its long side parallel to the spread in color of the turn-off region i.e. perpendicular to the TO of the isochrones, as displayed in Figure 3.3.1, then I applied a rotation to both color and magnitude of TO stars, moving to a frame with the x-axis parallel to the long side of the rectangle, and the y-axis perpendicular to it. Hereafter I will refer to the rotated color and magnitude as X and Y. In such frame the spread in color of the CMD turn-off is then just almost equal to the x spread. By choosing the long side of the rectangle as parallel as possible to the spread of the TO and rotating the region I obtained a reference frame in which the TO of an isochrone of a given age is almost a vertical line, which simplifies the next part of the procedure

II *Age of TO stars.* To find the age of each star I first find the x-coordinate of the isochrones in the grid corresponding to the y-coordinate of the i^{th} star, creating a set of couples $(x_{iso,j}, age_j)$. Then, I fitted the x_i-coordinate of the star considering the age of every isochrone and found the age of the star T_{star}. Every step of the procedure is shown in Figure (3.3.1). Panel (a) is the CMD of the cluster region with the grid of isochrones over-plotted. Panel (b) shows the selected TO stars (in red in panel (a)) in the X-Y plane and as expected their distribution is almost vertical. Finally panel (c) is age vs. X, i.e. rotated color. Dashed lines in panel (b) and (c) represent the 10^{th} and the 90^{th} percentiles of the color and age distribution, the latter used to compute the Δage parameter.

III *Some details on the selection of TO stars.* As said before, the rectangle is chosen with the long side as perpendicular as possible to the isochrones, in order to correctly estimate the age dispersion. Its upper side is instead selected avoiding the hook, visible in the border isochrones in Figure 3.3.1. In order to avoid degeneracy in age, isochrones have been cut right below the hook, so that every line intersect just once the upper long side of the parallelogram. This cut let us treat the relation between position in the TO region and star age as biunivocal.
Finally I tried to minimize the influence of binary systems considering that MS equal-mass binaries are distributed 0.75 mag above the MS, and choosing the rectangle just above this line.

IV Δage *determination.* Once the age for every TO star has been derived, I computed the Δage as the difference between the 10^{th} and the 90^{th} percentiles of the distribution. This is not a random choice. In previous works, **(Gooudfroij et al. 2014,2017)** has used the width of the age distribution at 20% of its maximum value ($W20$), or the Full Width at Half Maximum (FWHM), or in other words the 68^{th} percentile of the distribution, instead of the one adopted here to infer the age spread of the cluster. However, I will show that the age distributions of stars are not always gaussian-like, and they often show different degree of bimodality and/or extended tails. Because of these features, I will prove that the 68^{th} percentile is not optimal in estimating the cluster age variation.

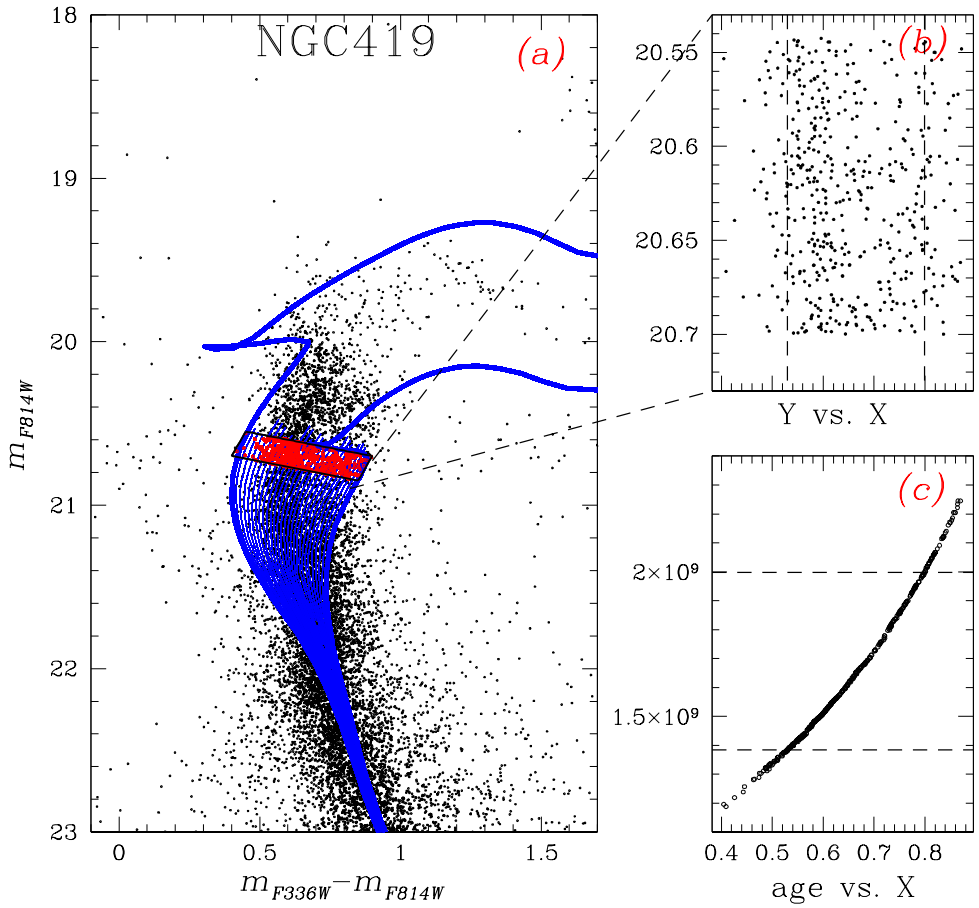

Figure 3.3.1: Panel (a) shows the CMD with isochrones over-plotted and red dots are stars selected in the TO region. As we can see some of the hooks intersects the parallelogram, leading to a possible degeneracy in age if not cut. Panel (b) shows X and Y of TO stars in the rotated frame of the and dotted line represents the 10^{th} and the 90^{th} percentiles of the distribution. Finally panel (c) is age in yrs vs. x-coordinate, or "color" of TO stars, and again dotted line are 10^{th} and 90^{th} percentiles.

NGC 419 age distribution for example (Figure 3.3.2) shows an extended tail toward older ages. The FWHM computed as $2\sqrt{2\ln 2}\sigma$ where σ is in turn the 68^{th} percentile of the residuals from the median value, does not describe well its age spread, since it does not account for this tail. Obviously the difference between the two estimators depends on the shape of the distribution itself and its deviation from gaussianity. Here I show some examples of distributions, again focusing on the difference between the Δage and the FWHM.

We see in Figure 3.3.3 that in the case of NGC1783 with an age of 1.9-2 Gyr the two estimators are almost identical because TO stars show a continuous spread in the CMD, producing a gaussian-like distribution. On the other hand, the cases of NGC411 and NGC1831 in Figure 3.3.4 are a completely different matter. As we can see their distributions are not just broadened, but they show a long tail towards older ages that is completely neglected by the FWHM. In these cases the

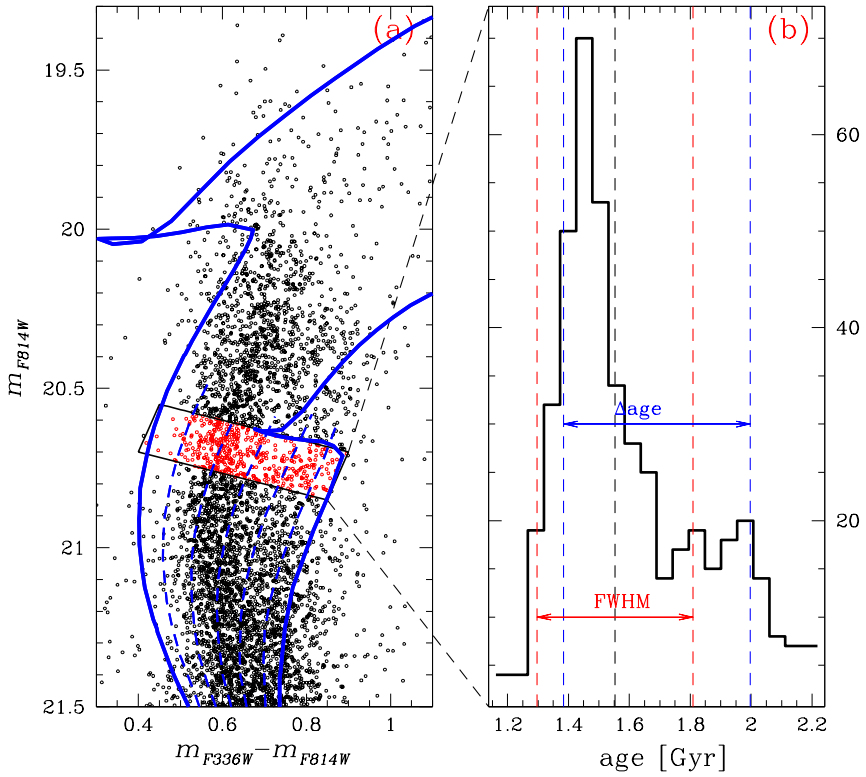

Figure 3.3.2: Panel (a): zoom of the TO region in NGC419 with some of the isochrones overplotted. Panel (b): age distribution of TO stars. Vertical black dashed line is the median age ($t = 1.5Gyr$), blue dashed lines are 10^{th} and 90^{th} percentile of the distribution and red dashed lines show the FWHM of the distribution.

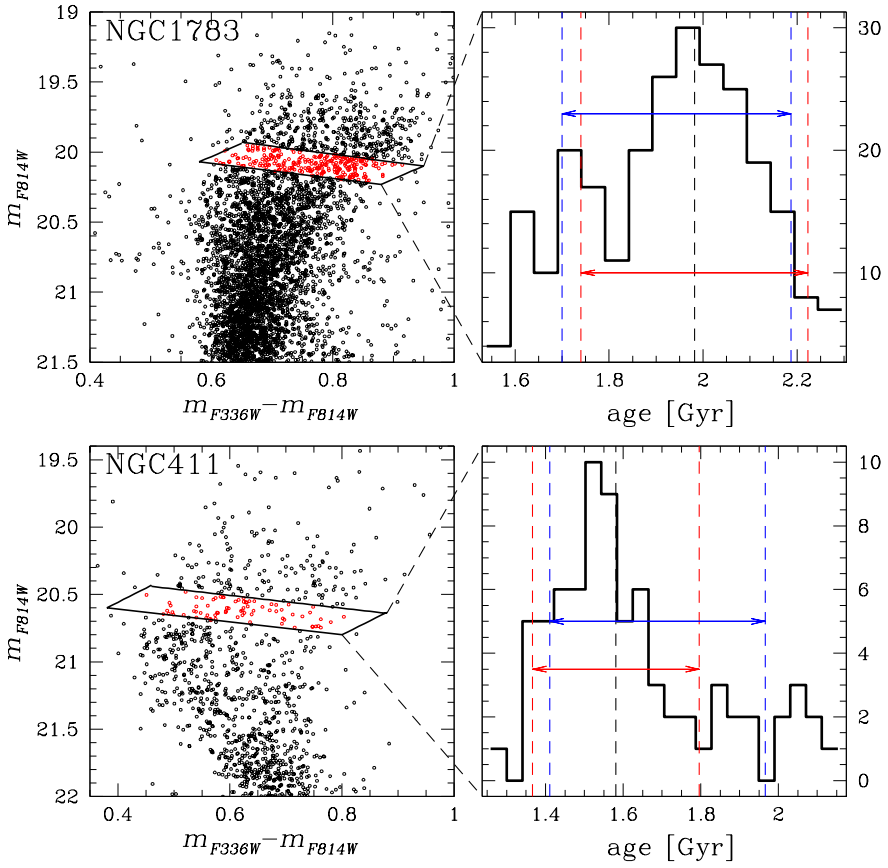

Figure 3.3.3: Same as Figure 3.3.2 for NGC1783 and NGC411. The first cluster shows a broadened distribution, comparable with a gaussian, and it is well described by both the FWHM and the Δage. NGC411 instead, has a distribution with an extended tail, and the Δage is by far a better estimator.

Cluster	date	camera	Filter	exp time	# images	GO	PI
KMHK250	2011,Oct,13	ACS/WFC	F814W	720	3	12257	L. Girardi
	2011,Oct,13	ACS/WFC	F435W	700	2	12257	L. Girardi
	2011,Oct,13	ACS/WFC	F555W	700	2	12257	L. Girardi
NGC265	2004,Nov,8	ACS/WFC	F814W	560	2	10126	E. Olszewski
	2004,Nov,8	ACS/WFC	F435W	440	1	10126	E. Olszewski
	2004,Nov,8	ACS/WFC	F555W	560	2	10126	E. Olszewski

Table 3.2: Description of the data

Δage better represents the age spread in the CMD.
In the case of NGC1953 the distribution is not widened, but shows a complete bimodality, which again does not affect the FWHM, while it is perfectly described by the Δage.

V *Boot strapping.* In less massive clusters the TO region is poorly populated, and thus the sample is affected by low statistics. In order to derive a more robust result I adopted the boot strapping procedure in computing the age difference, and its error. Once determined the age distribution, this is copied a 1000 times, creating a much larger sample (namely V) with dimension $N = 1000 \cdot n$, where n is the number of TO stars. Then a set of N random number between 0 and 1 is generated, and sorted in increasing order with the extended dataset. Finally the first n values of V are selected and $(\Delta age)_i$ is computed. This is repeated a 1000 times, creating a Δage distribution with dimension 1000, from which the final value is computed as the median value, and its error as the 68^{th} percentile of the residuals distribution. In this way I avoided results compromised by low statistics, which could have affected the final analysis.
As a byproduct of the age distribution computation, in this work I also determined the age of 27 Magellanic Cloud clusters, some of these for the first time. Final results are listed in Table 3.1.

3.4 First Time Analyzed Clusters

I dedicated a stand-alone section for the two newly analyzed clusters. Both of them present some peculiar and important features. Interestingly, the first one has never been studied before. In table 3.2 I give the general information relative to the dataset used in the data reduction of the two clusters.

3.4.1 KMHK250

KMHK250 is an open cluster located in the Large Magellanic Cloud. It's extremely low mass makes this object a really interesting case for our analysis. In fact, given its mass, it could not in principle retain the gas necessary to lead to a second star formation episode, or to a prolonged star formation, and therefore the presence of an eMSTO could add an important piece to the Magellanic Cloud multipopulations puzzle, in favor of the rotational scenario.
I used the procedure described in chapter 2 to reduce HST archive images in ACS/WFC *F435W*, *F555W* and *F814W* for this cluster.
Figure 3.4.1 shows the field of view with cluster and reference field used for the statistical subtraction, respectively in red and blue. In order to determine the radius of the cluster, since its looseness prevented the "by-eye procedure", I computed the density curve finding the distance from the center at which it became almost constant.

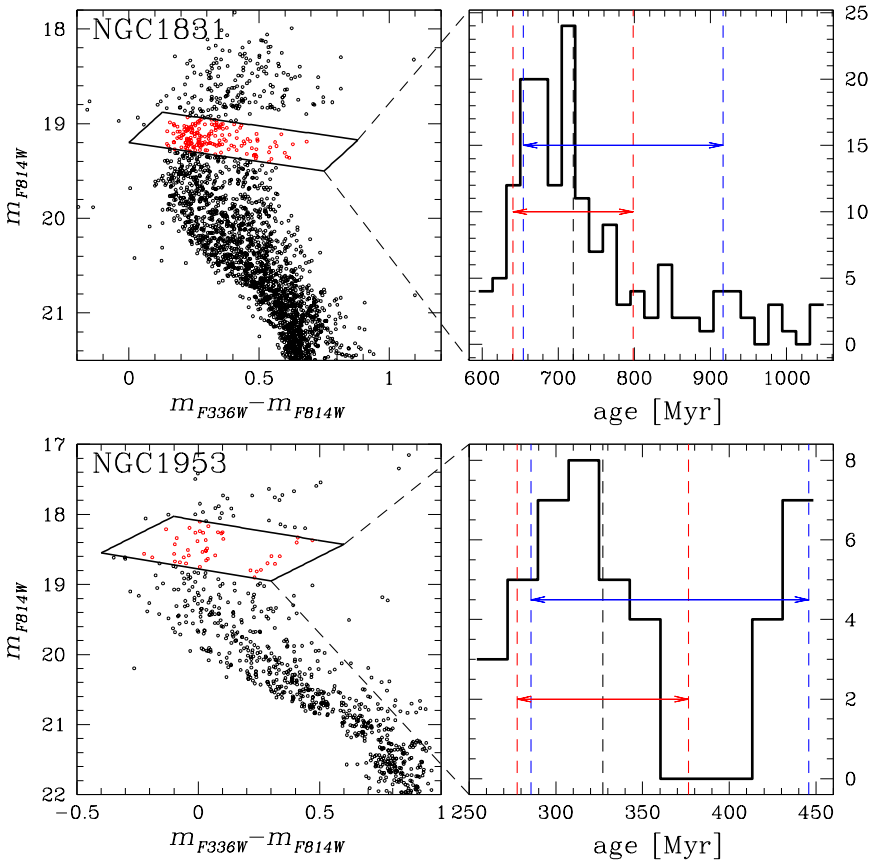

Figure 3.3.4: Same as Figure 3.3.2 for NGC1831 and NGC1953 both in the LMC. The first one shows a prolonged tail which is not accounted for by the FWHM, while the second one has a perfect bimodal age distribution, which again is well described by the Δage parameter but not by the FWHM.

Once determined the radius I proceeded with the statistical subtraction of the field, thus creating a clean CMD. However since cluster star density is not much greater than field star density the decontaminated CMD presents some holes and clumps in its MS, as in Figure 3.4.4. As shown in Figure 3.4.3, the low MS of the CMD of the cluster region is not much different from that of the CMD of stars taken from 4 random regions far from the cluster center. However, we can confidently say that the contamination from field stars is almost negligible in the TO region, in which we are interested in this work.

Figure 3.4.3 shows hints of the presence of an eMSTO, which cannot be attributed to field contamination, nor to the presence of binary/differential reddening and it is not compatible with a single isochrone. This is clearer in Figure 3.4.4, where the TO is "fitted" with two Padova isochrones of ages 1.5 and 1.85 Gyr, computed for a metallicity of Z = 0.006.

Measuring the TO age spread with the procedure just described I find a Δage of almost 500 Myr, which is near the maximum measured age spread. So, even if the analysis of this cluster's TO region has been the most difficult and uncertain, given its looseness and low statistics, I can confidently say that the TO region is compatible with an eMSTO, and this result alone poses some doubt on the "age-spread" scenario. Recalling the age spread vs. mass relation, in Figure 1.2.4 from [Goudfrooij et al., 2014], KMHK250 mass

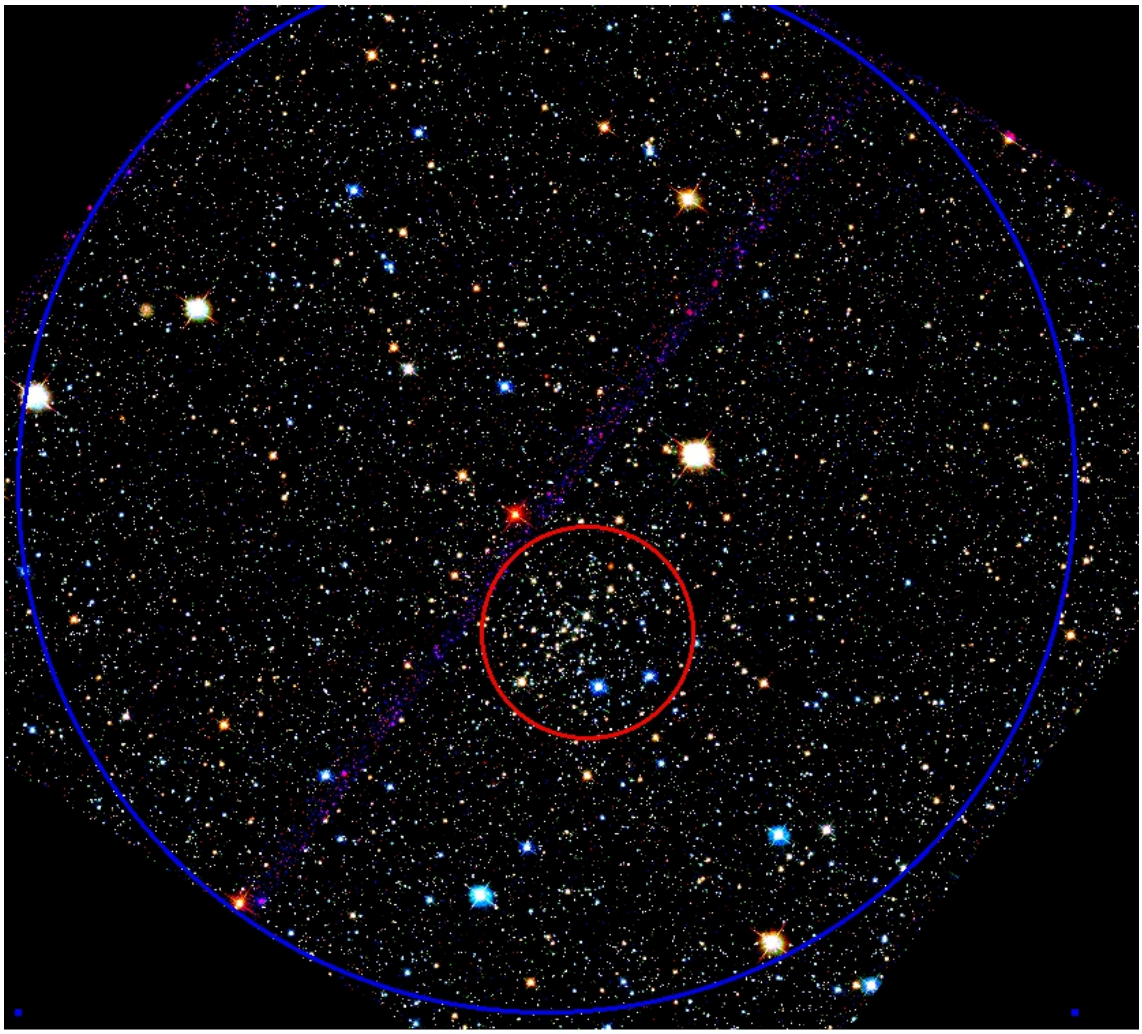

Figure 3.4.1: Trichromatic stacked image of KMHK250

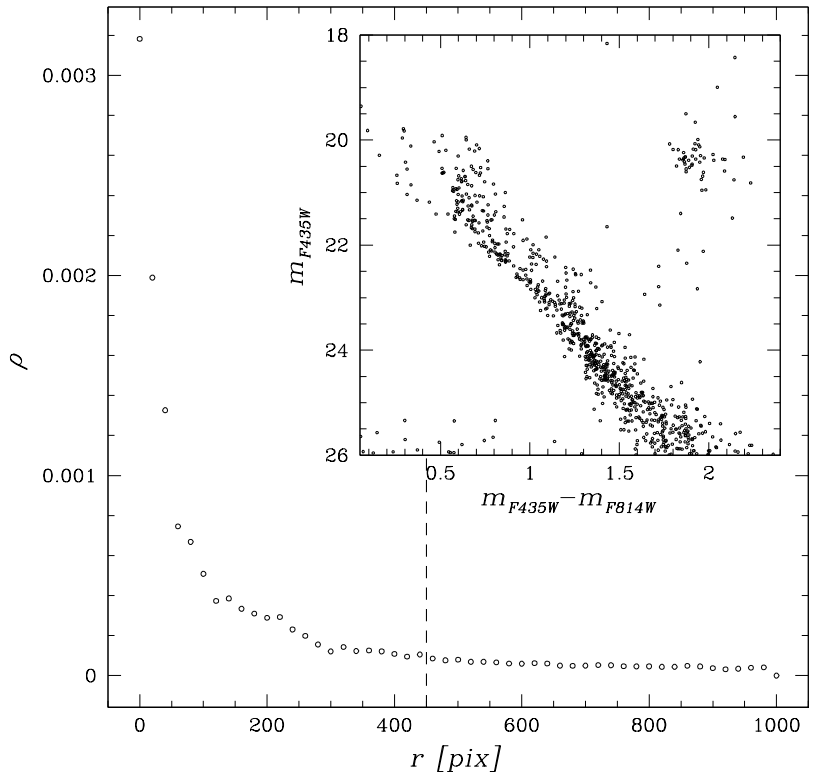

Figure 3.4.2: Density curve for the region within 1000 pixels from cluster center. The panel inside it shows the CMD of the region within the radius determined, corresponding to the black dashed line (450 pixels).

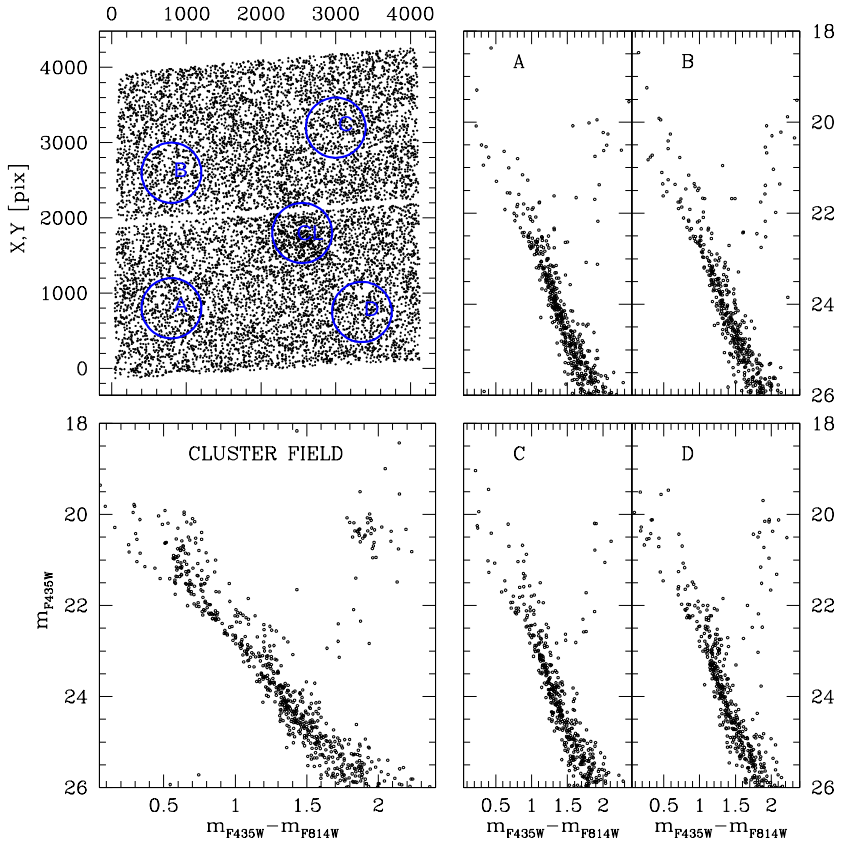

Figure 3.4.3: Comparison between the CMD of the cluster field and of four reference fields. The red circle is the cluster field with a radius of 450 pixels while the blue ones are the reference fields with the same radius as the cluster.

is much lower, by at least one order of magnitude, than the minimum mass required to host multiple stellar populations, and does not follow that relation. One possibility could be that this cluster lost most of its mass after the second star formation episode, and what we look at today is just the remnant of bigger cluster. However another possible explanation for this result could be that another physical phenomenon is responsible for the observed age spread.
Concluding, this cluster alone puts on the edge the age-spread scenario, testing one of its limits, and pushing toward some different mechanism responsible for the age spread in the cluster TO.

3.4.2 NGC265

NGC265 (figure 2.2.6) is a SMC open cluster located in the constellation Tucana, with coordinates : RA 00 47 11.4 DEC -73 28 37. For this cluster I downloaded images in ACS/WFC *F435W*, *F555W* and *F814W* filters from the HST archive. Interestingly, this object was already studied in [Chiosi and Vallenari, 2007], who did not report any evidence for multiple stellar populations.
I re-analyzed the data using the most-advanced technique described in section 2 finding some different and amazing results.
In panel (a) of Figure 3.4.5 is shown the CMD fitted with two non rotating Padova isochrones with different ages, and panel (b) is a zoom of the split MS of NGC265, in

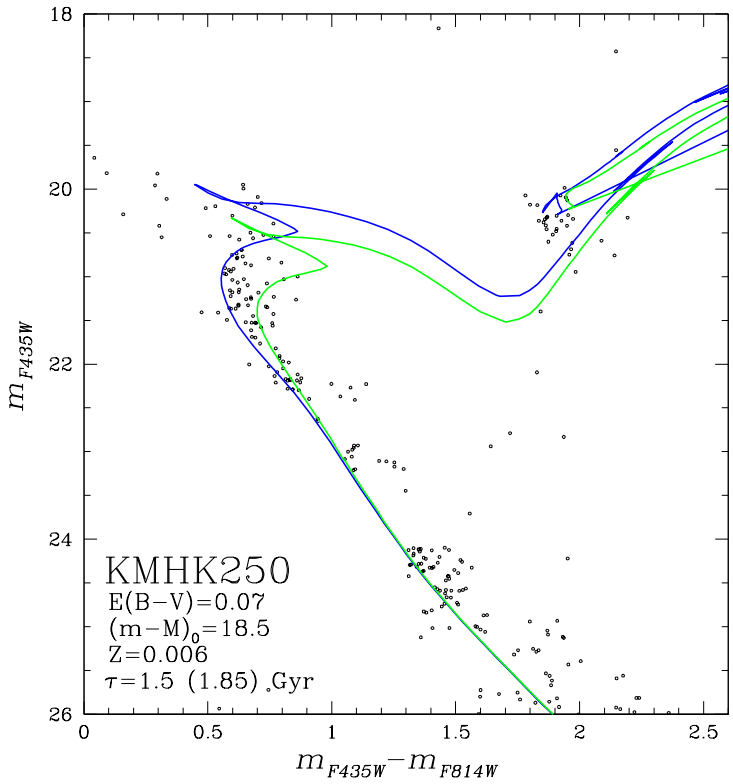

Figure 3.4.4: CMD of KMHK250 with non rotating isochrones for two different ages, from [Marigo et al., 2017].

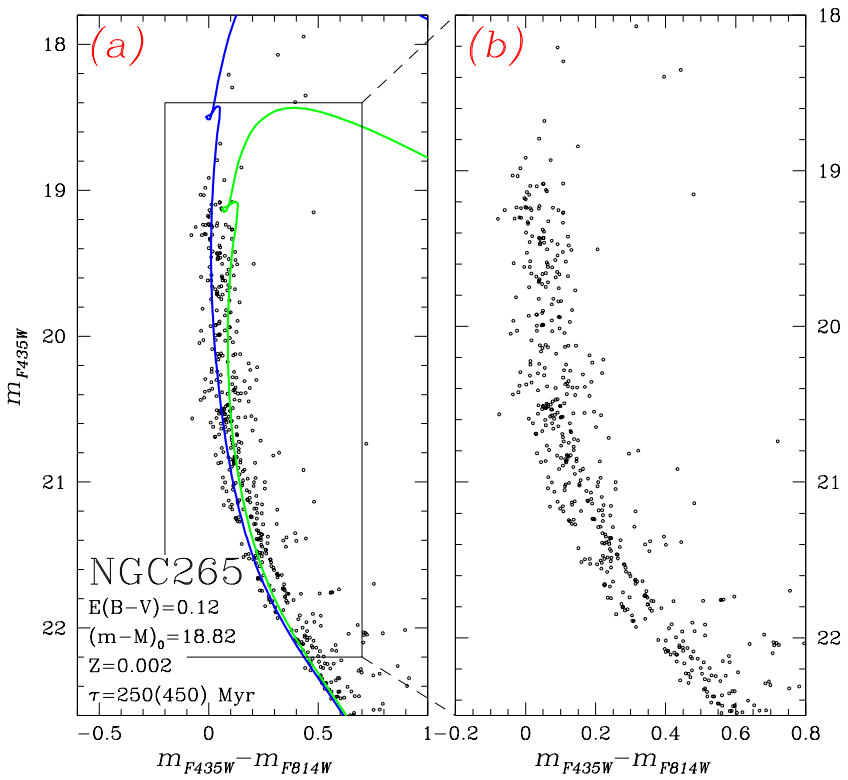

Figure 3.4.5: Panel (a) : calibrated CMD of NGC265 with two Padova isochrones from [Marigo et al., 2017] superimposed. Panel (b): zoom of the split MS of NGC265.

which the eMSTO and the split MS are more clear. This new split MS is a major finding of this work and will be analyzed, as in [Milone et al., 2018], determining the population ratio between the red and blue MS stars. Even if the filters combination of this CMD is not the best one to highlight the split MS (It is more visible in WFC3/UVIS$F336W$ and $F814W$ filters)we see that there is a good separation of about 0.1 in color.
Here I analyzed it with the same procedure described above, determining its age and finding its age spread. What I find is an extremely high value of the Δage, of almost 200 Myr, which quite large value for a cluster of $\sim$ 330 Myr. This could be caused by the fact that the images I analyzed are few archive images (Table 3.2), and they are not of the best quality. Thus the result could be slightly altered, and in particular the age spread could be overestimated.

CHAPTER 4

Results and Discussion

The procedure described in Section 3.3 has been extended to all the clusters to infer their age and the age spread, which is needed to reproduce their eMSTOs. I used two quantities which are indicative of the age spread, namely the Δage parameter, defined as the difference between the 10^{th} and the 90^{th} percentile of the age distribution, and the FWHM, which is defined as 2.35σ, where σ is the 68^{o} percentile of the age distribution. As a byproduct, I estimated the distance modulus of each cluster and the average reddening in the analyzed field of view. These results are summarized in Table 4.1. I find that the analyzed clusters span an age interval between $\sim$ 40 Myr and $\sim$ 2.8 Gyr Myrs and that the age spread, Δage, ranges between $\sim$ 20 and $\sim$ 600 Myrs. NGC 419 is the cluster with the maximum age spread of 615 Myr, while NGC 1805 exhibits the smaller value of Δage ($\sim$ 20 Myr).
In this chapter I investigate the relation between the cluster age and the age spread and I will discuss these findings in the context of the main scenarios for the formation of MPs in young and intermediate-age GCs.

4.1 Results

The relation between the age spread and the cluster age is shown in Figure 4.1.1, where I plot the derived values of Δage (upper panel) and FWHM (lower panel) as a function of age. Blue and green dots correspond to LMC and SMC clusters, respectively. Top panel shows a quite peculiar relation, as the age spread increases almost linearly with cluster age, i.e. old clusters have, on average, a larger age variation than young clusters. This age spread reaches its maximum value for cluster ages between $1.5Gyr$ and $1.8Gyr$ and then drops steeply for older ages. The same trend is observed in the logarithmic plot, in Figure 4.1.2, where the drop of the age difference is less evident because of the logarithmic scale.
A visual inspection of the two panels of Figure 4.1.1 reveals that the data follow similar trends in both the Delta age vs. age and in the FWHM vs. age planes. But, while in the Δage-age relation the linear part is quite narrow, in the FWHM-age one I note a larger dispersion of the points. In fact, as shown in Figure 3.3.3 and 3.3.4 the FWHM parameter is less sensitive to extended tails and/or bimodal peaks in the pseudo-age distribution than Δage.
For example, NCC1783 which has a Gaussian-like age distribution, has the same relative location in the Δage-age and FWHM-age relations. However this is not true for the other three highlighted clusters, whose distributions deviates from gaussianity. The fact that the FWHM has a poor sensitivity to the tails of the distribution may translate in a

Cluster	$Age[Myr]$	$\Delta age[Myr]$	$FWHM[Myr]$	$(m-M)_0$	$E(B-V)$	$R_{cf}[arcsec]$
KRON 34	840 ± 10	380 ± 55	390 ± 70	18.80	0.07	20
NGC 152	2100 ± 10	300 ± 60	270 ± 60	18.80	0.03	24
NGC 294	690 ± 25	300 ± 35	300 ± 50	18.80	0.10	22
NGC 265	330 ± 20	230 ± 20	235 ± 25	18.85	0.12	25
NGC 330	40 ± 2	40 ± 6	25 ± 5	18.80	0.11	24
NGC 411	1580 ± 20	545 ± 80	415 ± 65	18.85	0.11	28
NGC 419	1550 ± 10	615 ± 15	510 ± 40	18.85	0.13	56
NGC 1651	2165 ± 20	320 ± 30	285 ± 30	18.48	0.08	32
NGC 1755	87 ± 3	45 ± 7	35 ± 6	18.35	0.13	30
NGC 1783	1980 ± 20	480 ± 30	470 ± 10	18.45	0.04	50
NGC 1801	305 ± 6	125 ± 20	80 ± 25	18.40	0.16	28
NGC 1805	40 ± 3	20 ± 4	15 ± 5	18.35	0.10	22
NGC 1806	1900 ± 30	550 ± 25	530 ± 30	18.45	0.05	48
NGC 1818	50 ± 2	40 ± 9	35 ± 5	18.40	0.10	40
NGC 1831	720 ± 6	260 ± 25	160 ± 14	18.35	0.07	36
NGC 1846	1820 ± 8	555 ± 20	505 ± 25	18.35	0.04	58
NGC 1850	90 ± 4	45 ± 3	40 ± 5	18.35	0.15	40
NGC 1852	1605 ±	470 ± 40	470 ± 45	18.55	0.08	26
NGC 1856	340 ± 5	140 ± 20	125 ± 14	18.28	0.19	20
NGC 1866	180 ± 3	100 ± 8	90 ± 10	18.35	0.13	32
NGC 1868	1050 ± 10	340 ± 60	240 ± 30	18.45	0.13	40
NGC 1953	330 ± 8	160 ± 10	105 ± 30	18.40	0.16	24
NGC 1978	2685 ± 8	375 ± 30	300 ± 20	18.42	0.04	34
NGC 1987	1060 ± 30	320 ± 40	290 ± 40	18.35	0.08	26
NGC 2164	120 ± 3	60 ± 8	60 ± 10	18.35	0.10	30
NGC 2173	1740 ± 30	550 ± 55	545 ± 40	18.35	0.11	32
KMHK 250	1540 ± 20	445 ± 80	305 ± 80	18.50	0.07	20

Table 4.1: Results of the analysis described in Chapter 3

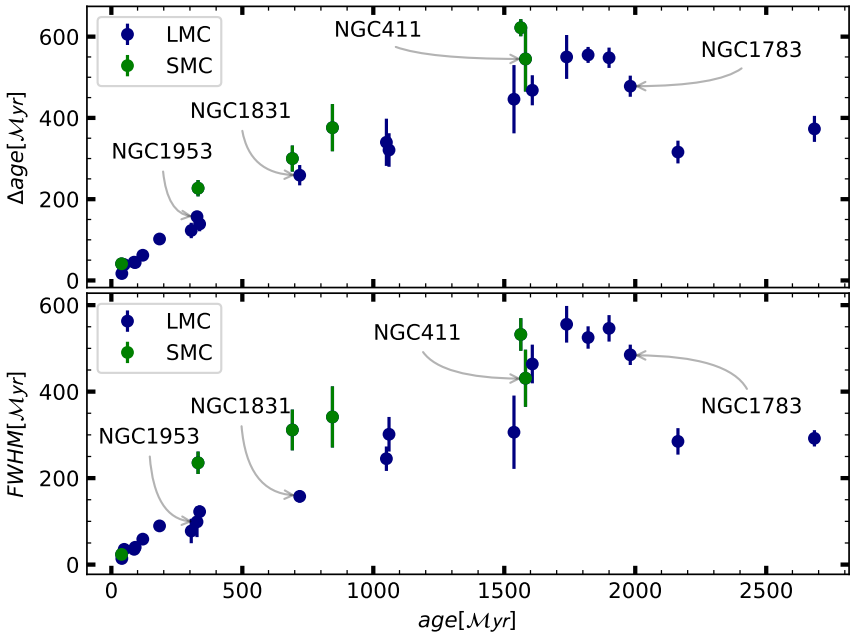

Figure 4.1.1: Age spread versus cluster age. Blue and green dots are respectively LMC and SMC clusters. The four clusters whose distribution has been presented in Section 3.3 are pointed out with arrows. The age spread has been plotted both as Δage (top panel) and FWHM(bottom panel).

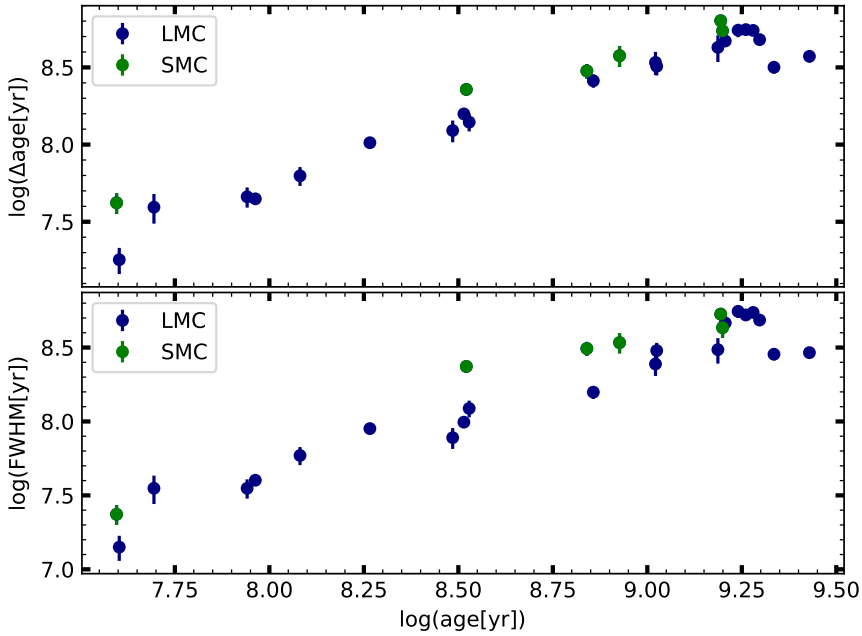

Figure 4.1.2: Same as figure 4.1.1 in logarithmic scale.

widening of the relation, mostly in the linear regime.
Interestingly, in both the linear and the logarithmic relation, all SMC clusters have an age spread that is systematically larger than that of LMC clusters with similar age. It would be tempting to speculate that the large age spread of SMC cluster is due to the different metallicity between the Magellanic Clouds, or that the environment plays an important role in the whole multipopulations phenomenon, however we need first to understand which physical phenomenon is responsible for the observed age spread vs. cluster age relation.

4.1.1 Implications on the Multi-populations Scenarios

In the Chapter 1 I introduced two main scenarios that account for the eMSTO and the split MS in the CMDs of Magellanic Clouds YCs and IACs: the *age-spread* scenario and the *rotational* scenario. In the following I investigate the implications of the correlation plotted in Figure 4.1.1 with its implications on these two models.

Age spread **scenario**

Suppose here that the analyzed clusters experienced a prolonged star formation, and now host different stellar generations, which are then responsible for the observed eMSTO. We would expect to find that age variations are not related to cluster age, as there is no reason for a 1 Gyr cluster to have a smaller age spread than a 1.5 Gyr cluster. The age spread vs. age relation then would not be as narrow as the one in Figure 4.1.1, but more scattered, resembling a random relation. Even more difficult to explain would be the sudden drop of the age variation for cluster older than $\sim$ 1.8-1.9 Gyr.
Concluding, the peculiar shape of the relation proves that the presence of an eMSTO cannot be attributed solely to an age difference in cluster stars.

Rotational **scenario**

Another possibility is that the eMSTO is caused by the presence of coeval stellar populations with different and extreme rotation rates, for example a non-rotating population and a rotating one with $\omega = 0.9\omega_{crit}$, where ω_{crit} is the break-up rotation velocity. The simulated CMD of a simple population of stars with the same age and metallicity but different rotation rates exhibit the eMSTO, in close analogy with what we observe in Magellanic-Clouds clusters. Figure 4.1.3 shows the (F336W − F814W) vs. F814W CMD of a simulation of 500 Myr-old cluster computed with the Geneva `SYCLIST` model. The simulated cluster hosts two coeval stellar populations with different rotation rates. Since all the simulated stars have the same age and chemical composition, the color and magnitude spread of the MSTO is entirely due to stellar rotation.
How would then the age spread vs. age relation appear if this eMSTO is interpreted as a physical age spread, and not as a consequence of rotation? To answer this question I applied the procedure described in Chapter 3 to the simulated clusters with different ages, composed of coeval stellar populations with different rotation rates, as the one represented in Figure 4.1.3.

4.1.2 Clusters Simulations

I simulated a sample of 13 clusters with metallicities equal to those adopted in this work (Z = 0.006 for the LMC and Z = 0.002 for the SMC) and with different ages, spanning from $\sim$ 30Myr to $\sim$ 1.25Gyr. These simulated clusters host two different coeval stellar populations, a non-rotating one and a fast rotating one, with $\omega = 0.9\omega_{crit}$. Simulations for older clusters are not available and so I couldn't reproduce the whole observational regime.
This simulations have been computed with the Geneva `SYCLIST` web tool (`https://obswww.unige.ch/Recherche/evoldb/index/`) and have been transformed into the HST

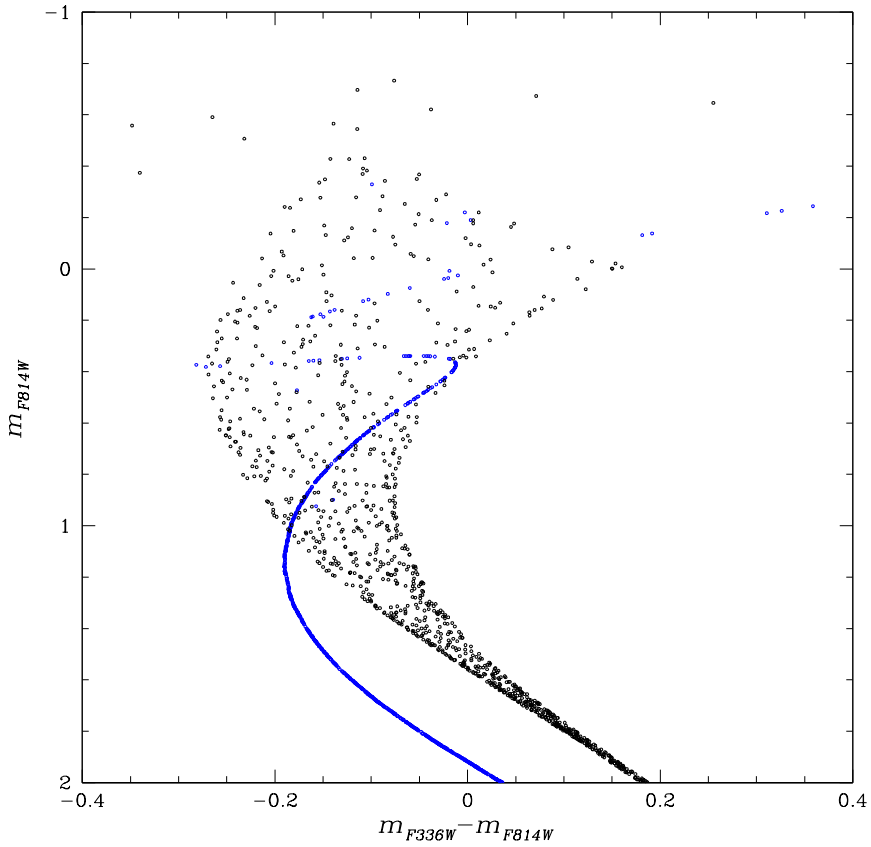

Figure 4.1.3: Simulation of a 500 Myr-old cluster hosting two coeval stellar populations with different rotation rates, computed with the Geneva `SYCLIST` model. Blue open dots are non rotating stars and black dots are stars rotating with $\omega = 0.9\omega_{crit}$.

observational plane using the model atmospheres by Castelli & Kurucz (2003), convolved with the HST filter transmission curves by courtesy of Dr. Marcella Di Criscienzo[1]. The adopted model accounts for a random distribution of the viewing angle, which alters the observations since the star, rotating, changes its shape deviating from sphericity and becoming oblate. As a consequence it develops polar temperature gradients. The stellar fluxes depend on the viewing angle with respect to the rotational axis. This effect is known as gravity darkening. The model includes also the effect of limb darkening, because of which the center disk of a star appears brighter than its limb.
I have then analyzed the simulated CMDs with the very same procedure described in Chapter 3 for real data, i.e. interpreting the spread TO as due to non-rotating stars with different age. Specifically, for each simulated cluster I derived the age and the age spread by fitting non-rotating isochrones of different ages to the simulated CMD. I reproduced the age spread vs. cluster age relation and finally compared this theoretical relation with the one computed from real clusters (Figure 4.1.1).
The simulation of a 250Myr-old cluster is shown in Figure 4.1.4. The panel on the left is the plain CMD of the simulated cluster, where blue points are non rotating stars and black ones are fast rotators, with $\omega = 0.9\omega_{crit}$. In the right panel I over-imposed on the CMD, the best-fit non-rotating isochrones from the Padova database [Marigo et al., 2017]. Similarly to what I have done in the analysis of the observed CMDs, I used red-MS stars to infer the best-fit parameters. I repeated the procedure for every simulated cluster, using

[1]Istituto Nazionale di Astrofisica (INAF), Osservatorio di Roma

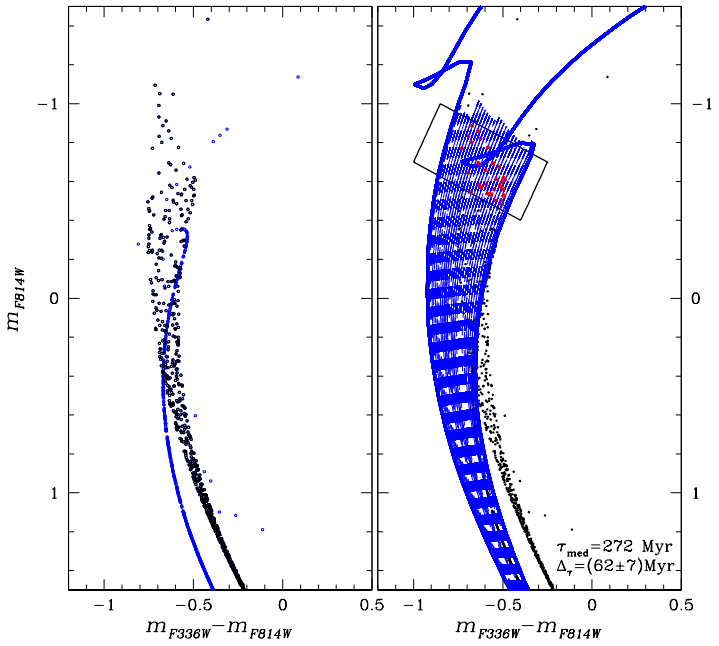

Figure 4.1.4: Same as Figure 3.3.1 for the simulation of a 250 Myr-old cluster with fast rotating ($\omega = 0.9\omega_{crit}$, black points) and non rotating stars (blue points).

F336W and F814W filters, in order to match the photometry of most clusters.

4.2 Discussion

The results of the analysis of the simulations are shown as red triangles together with the "observations" in the linear regime ($age \lesssim 1.8Gyr$), in Figure (4.2.1). The age variation increases with the age of the simulated clusters almost linearly, similarly to what we observe for real clusters (blue and green points). This result suggests that, if the spread due to rotation is mistakenly interpreted as a physical age spread, the age spread vs. age relation have the same trend as the observed one. The fact that the analyzed GCs follow a similar trend as the simulated clusters in the Δage vs. age plane demonstrates that rotation plays a major role in determining the eMSTO.

Since for ages less than $\sim 1.8Gyr$ the relation is almost linear, I fitted the two datasets with a straight line, using a linear least square interpolation. Red and blue lines in Figure 4.2.1 are the results of the interpolation. The slope, a, and intercept, b, of the straight line that provides the best-fit with the observed data and the simulations are:

$$\text{data: } \begin{cases} a = 0.31 \pm 0.02 \\ b = 40 \pm 15 \end{cases} \qquad \text{simulations: } \begin{cases} a = 0.32 \pm 0.01 \\ b = -11 \pm 5 \end{cases}$$

As we can see from panel (a) of Figure 4.2.1 The two lines have the same slopes at 1-σ level, while the intercept differs by more than 3 σ. The shift between the two fitted relations is however expected because photometric errors are not included in clusters analysis, and therefore the measured age spread is greater than its real value, while simulations do not have observational errors, and the relation lies $\sim$ 50Myr below the

observational one. We can conclude that the similar trend of the two relations shown in Figure 4.2.1 proves that rotation plays a major role on the color and and magnitude of eMSTO stars.

From this analysis, I can conclude that it is unlikely that young and intermediate-age clusters in the LMC and the SMC exhibit large age spread. Nevertheless, it is not clear whether age variations, in addition to rotation, are responsible for the eMSTOs or if the eMSTOs are solely due to rotation. In order to achieve this result I have analyzed the deviation and dispersion from the observational relation.

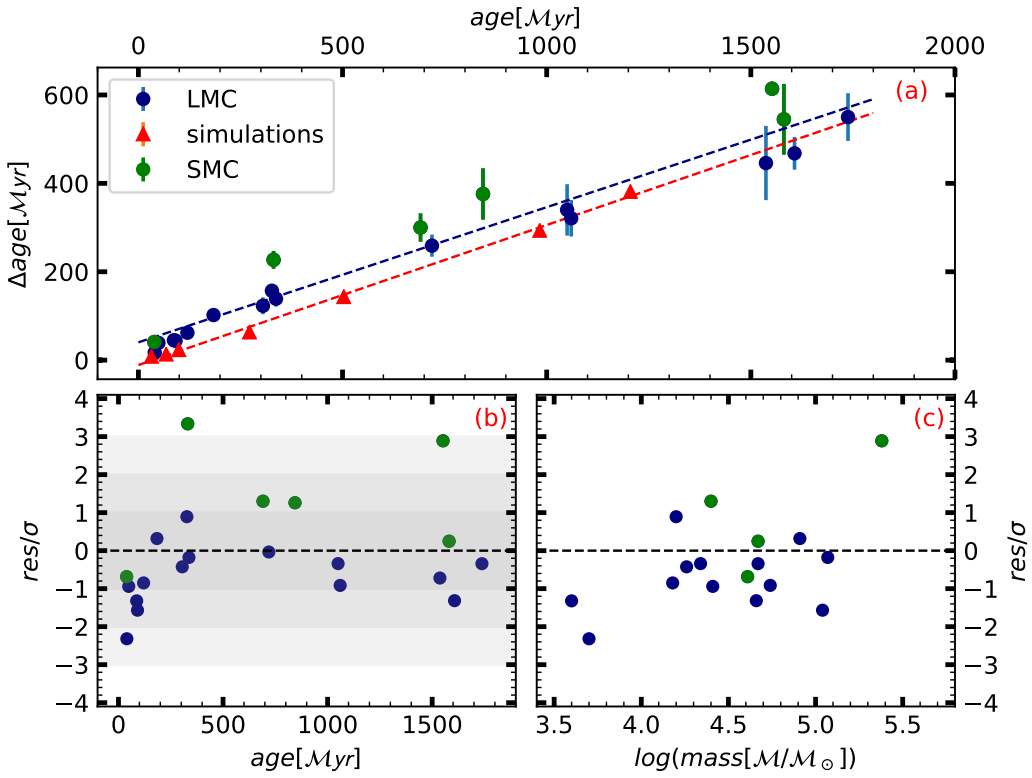

Figure 4.2.1: panel (a): observational data for clusters younger than 1.8 Gyrs are represented as filled blue dots, while filled red triangle are the results computed from the simulations in F336W and F814W filters for clusters with metallicity Z = 0.006, equal to that used for the LMC. Red and blue dashed lines are respectively the theoretical relation and the observational one, computed as linear least squares interpolation. Panel (b) shows the residuals of the data, computed as the difference between the age difference and the blue dashed line, normalized over their σ in relation to cluster age. Panel (c) shows the same quantities in relation to cluster mass.

Panels (b) and (c) of Figure 4.2.1 show respectively the residuals of the relation normalized over their σ in relation to cluster age and cluster mass. The residuals and their errors are computed using equation 4.1. These two plots give, in a direct and immediate way, the dispersion of the points in terms of their sigma, or in other words they tell us to which degree the age spread is consistent with the rotational scenario, and therefore if any cluster is compatible with hosting stars with different age, in addition to coeval stars with different rotation velocities. In particular

$$res_i = (\Delta age_i - (m * age_i + q)) \qquad \sigma^2_{res,i} = \sigma^2_\Delta + age_i^2 \sigma^2_m + \sigma^2_q \tag{4.1}$$

Almost every LMC cluster, young or intermediate-age, is compatible with the relation within 2σ, with the exceptions of NGC 1805 which lies slightly below the 2σ region. This discrepancy is probably due to the few number of stars in the TO region, which could affect the age spread determination. I can thus state that LMC clusters are in agreement with a model in which clusters have coeval stellar populations with different rotation rates. SMC clusters (green dots) however, lie systematically above the best fit relation, having a larger age spread with respect to their LMC companions.
Concerning IACs, we see from panel (b) and (c) that they too are compatible with the theoretical relation within 2σ. The only exceptions is the SMC cluster NGC419 whose age spread is much larger than expected. Again deviations could be due to the different metallicity or it could mean that this cluster host different stellar generations in addition to coeval rotating and non-rotating stars. Anyway, in the latter case, the real age spread would be, at most, a 100Myr, which is by far less then what expected from previous works in literature.
An important result that we can deduce from Figure 4.2.1 is that there is no apparent relation between the deviation from the expected relation and cluster's main parameters, such as age and mass.
I will now analyze other possible causes for deviations from the theoretical relation, in order to understand the physical phenomenon/s responsible for the pseudo age spread.

4.2.1 Dependence of *Age spread* vs. *Age* Relation from the host galaxy

Why do SMC clusters show larger age spread than LMC clusters? The first guess is that this difference is due to the different metallicity of the two galaxies ($Z_{SMC} = 0.002$ and $Z_{LMC} = 0.006$). Metallicity could in fact play an important role in the rotation of the stars and in the possible braking process, leading to some differences in the observed pseudo age spread. One way to estimate the contribution of the metallicity is to compare simulations of clusters with $Z = 0.006$ and $Z = 0.002$, composed again of two coeval stellar populations with extreme rotation velocities.
I computed the age spread for 6 simulated clusters with $Z = 0.002$, this time with a maximum age of 1 *Gyr*, and I built the theoretical relation. Finally, I compared this relation with the one computed for the metallicity of the LMC.
Figure 4.2.2 shows that again the pseudo age spread increases with cluster age, but this time the slope of the best fit line for $Z = 0.002$ is shallower than that relative to a metallicity of $Z = 0.006$. However, this difference is likely due to the lack of a simulated cluster with age ~ 1.25 Gyr at $Z = 0.002$. If I in fact suppose to cutoff the data at 1 *Gyr*, then the slope of the two curves would be much more similar, and the relations almost identical.
If the two relations are quite similar then this means that the excess age spread in the SMC clusters have to be caused by some other physical phenomenon. In particular we see that there are two clusters that lie well above the relation, and whose distance is $\sim 3\sigma$: NGC 265 with an age of ~ 330 *Myr* and NGC 419, whose age is ~ 1.5 *Gyr*. Part of the excess spread of the young cluster is probably due to the fact that the data reduction has been done on few archive images, and therefore the resulting photometry is not as precise as that of the rest of the sample. There seems to be no reason instead for NGC419 to have such an age difference excess.

4.2.2 Dependence of *Age spread* vs. *Age* Relation from the filter

Since this dataset is quite heterogeneous, not every cluster has been analyzed using the same HST filters combination. In particular most of clusters younger than $\sim$ 1Gyr, taken from [Milone et al., 2018], and part of older clusters are all analyzed in HST WFC3/UVIS *F336* and *F814W*. There are however some clusters, like KMHK 250, NGC 265, NGC 1846, NGC 1783 whose images are taken with ACS/WFC *F435W*, *F814W* filters. In order to estimate possible differences between different filters combination I analyzed

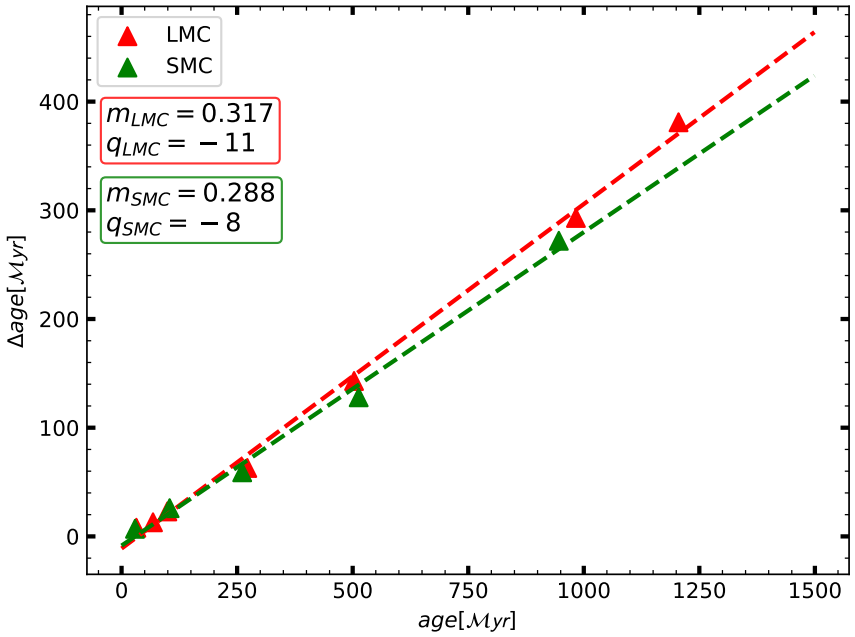

Figure 4.2.2: Theoretical relation for two different metallicities. Red triangles are simulated clusters with metallicity equal to that of the LMC (Z = 0.006) and green pentagons are simulated clusters with Z = 0.002, as the SMC. Dashed lines are the result of the linear least squares interpolation.

the same previous simulations, this time using ACS/WFC *F435W* an *F814W*, and I compared the two curves.

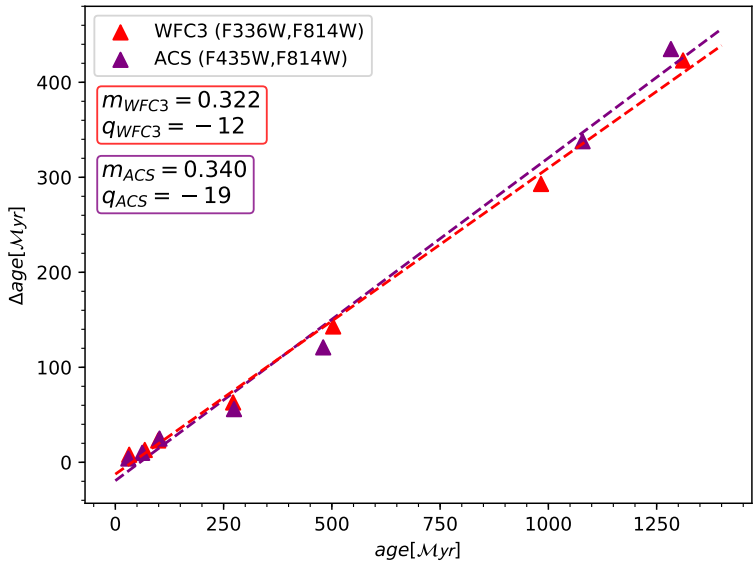

Figure 4.2.3: Theoretical relation for two set of filters. Red triangles are computed using WFC3/UVIS *F336* and *F814W* while purple ones with ACS/WFC *F435W* an *F814W*.

Results of this comparison are shown in Figure 4.2.3. It is evident that the two relations are quite similar and different filters combinations do not drastically alter the result.

4.2.3 Dependence of *Age spread* vs. *Age* Relation from the age distribution shape

So far I have analyzed the results considering only the Δage parameter and not the FWHM. In chapter 3 I showed the differences between the two parameters in relation to the shape of the cluster age distribution. In particular Figures 3.3.3 and 3.3.4 show how the FWHM does not describe well the age spread if the age distribution has an extended tail and/or if it is bimodal. This means that some of the computed FWHM values are underestimate the age spread of the cluster. For these reasons, computing the difference between the data and the fitted observational relation by using the FWHM values would not give useful insight on the physical mechanisms governing the age spread.

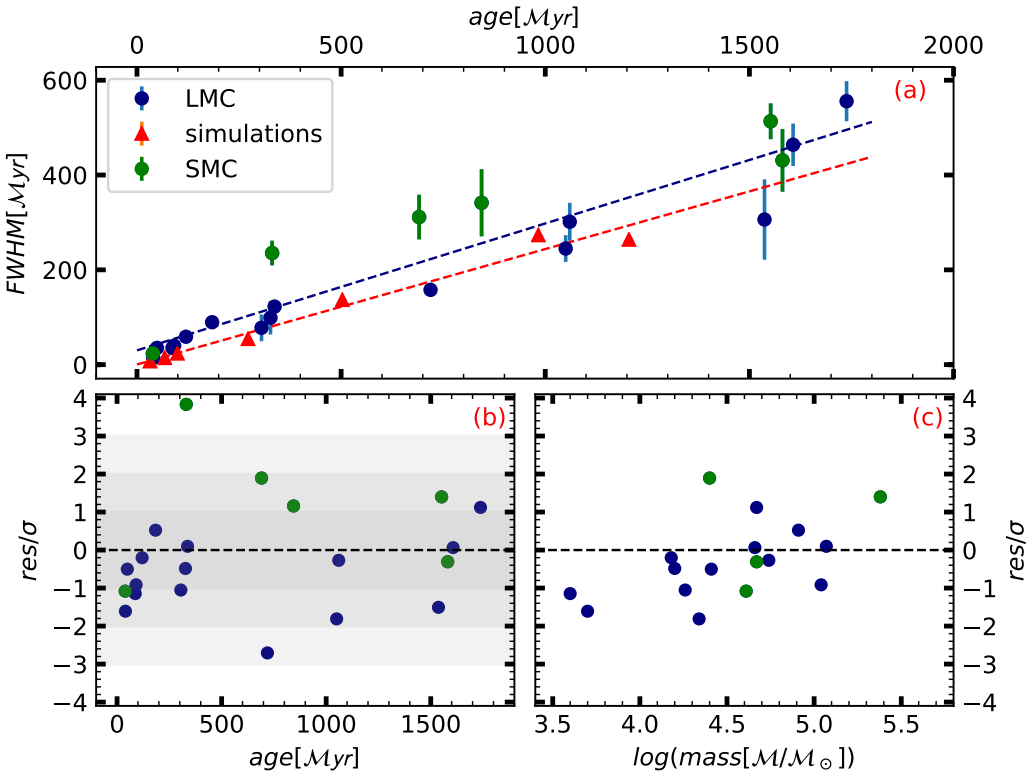

Figure 4.2.4: Same as Figure 4.2.1 using the FWHM of the age distributions instead of the Δage.

The same considerations are true for age distributions of simulated clusters, and in fact the relation is quite different from the one computed with the Δage parameter (see Figure 4.2.4). The residuals in panel (b) and (c) are again computed from the observational relations.

$$\text{data: } \begin{cases} a = 0.269 \pm 0.022 \\ b = 29 \pm 20 \end{cases} \qquad \text{sim: } \begin{cases} a = 0.244 \pm 0.012 \\ b = 0 \pm 11 \end{cases}$$

4.2.4 Dependence of the Pseudo-age Distribution from the parameters of the host cluster

It is natural now to wonder whether the age distribution behavior is due to some particular physical mechanism, and if so, if there is any correlation between the distribution shape and the cluster physical parameters, like its age or its mass.
The first problem to solve is how to treat the presence of possible bimodality in the pseudo-age distribution, and how to express it with a single parameter. In order to classify the shape of the distribution, and in particular its bimodality, I adopted the *BC* parameter, defined in equation 4.2,

$$\mathrm{BC} = \frac{\mathrm{m}_3^2 + 1}{\mathrm{m}_4 + 3 \cdot \frac{(\mathrm{n}-1)^2}{(\mathrm{n}-2)(\mathrm{n}-3)}} \tag{4.2}$$

where m_3 and m_4 are respectively the skewness of the distribution and its excess kurtosis. The value of the parameter is then compared with the critical value that would be expected for a uniform distribution (Equation 4.3); higher numbers point toward bimodality whereas lower numbers point toward unimodality.

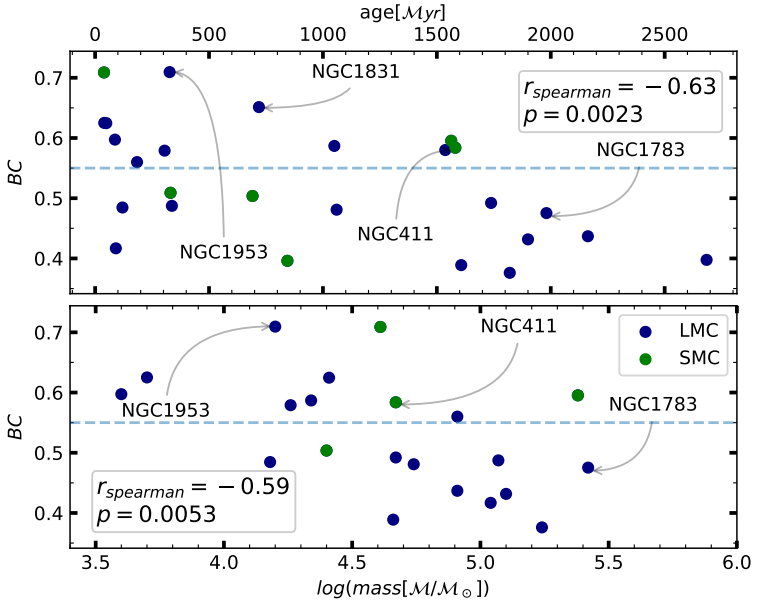

Figure 4.2.5: BC parameter versus cluster age and cluster mass. The four clusters described in Section 3.3 are highlighted, however in the bottom panel NGC1831 is missing since we do not know its mass. In both panels are shown the Spearman correlation coefficients ($r_{spearman}$) and the probability of uncorrelated data (p) with that Spearman coefficient.

$$BC_{crit} = 0.55 \tag{4.3}$$

This parameter however does not distinguish between a distribution with an extended tail and a bimodal one. After computing the *BC* parameter for every cluster we looked for a correlation with the cluster age or mass, which are the most straightforward candidates. We show the results in Figure 4.2.5. As in Figure 4.1.1, clusters whose age distribution is shown in section 3.3 are pointed by arrows and green dots are SMC cluster. In Figure 4.2.5 the bimodality parameter versus cluster age and/or mass is shown. To investigate the possible correlation between these quantities, I computed the Spearman correlation coefficient and the probability of uncorrelated data. The value of $r_{spearman}$ goes from

−1 for anti-correlated data to 1 for correlated data and values close to 0 imply non correlation. p instead is the probability of a random dataset to have a Spearman coefficient at least as extreme as the one computed. Our results are consistent with a hint of correlation between bimodality and cluster age and mass. However, this is just a first degree analysis that could be the first step in future studies regarding this phenomenon. Its comprehension could indeed shed light on the physical mechanism responsible for the braking of stars in clusters.

4.3 Comparison with Literature

I finally compared the results obtained in this work with the results present in literature. In particular I refer to the results obtained in [Goudfrooij et al., 2014],[Goudfrooij et al., 2017] and [Niederhofer et al., 2015].

4.3.1 *Age spread* vs. *Age* Relation

As found in previous works (see [Goudfrooij et al., 2017] and [Niederhofer et al., 2015], Figure 4.3.1) there is a linear relation between age spread and cluster age for cluster younger than $\sim 1.7 Gyr$, which is in agreement with the SYCLIST models of cluster populated by coeval stellar populations with a a range of rotation velocity.

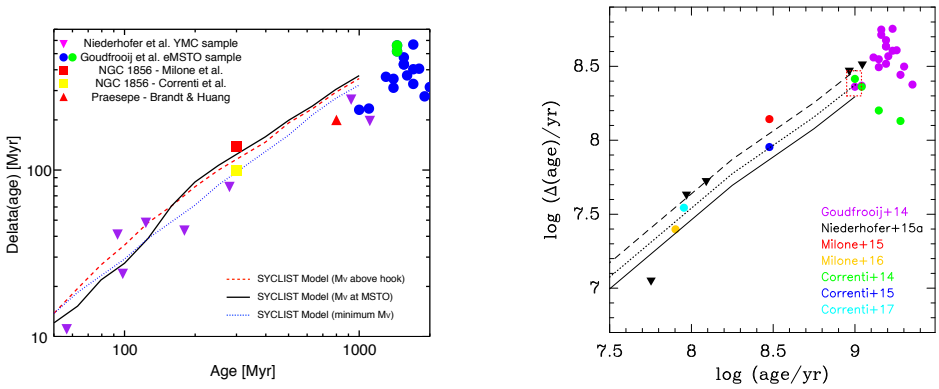

(a) *[Niederhofer et al., 2015]* (b) *[Goudfrooij et al., 2017]* .

Figure 4.3.1: *Age Spread* vs. *Age* from literature.

Although, differing from the conclusions of [Goudfrooij et al., 2017], my results show no need of introducing a real age spread of a few hundreds Myr in addition to the pseudo-age spread provided by the rotational model. Figure 4.2.1 shows in fact that most clusters lie within 1 σ from the expected relation, and therefore their age spread is consistent with rotation alone. The only cluster for which we are not able to determine the physical phenomenon responsible for the age spread in the TO region is NGC 419, whose Δage is almost 100 Myr larger than expected. Further analysis are required in order to disentangle the multipopulation phenomenon in this cluster.
The main difference between this work, and the two cited ones is that here I used a much larger sample of data, which includes both young and intermediate-age cluster, analyzed consistently with simulations. This means that the obtained results are not biased by the data analysis technique, as could be for different datasets.

4.3.2 *Age spread* vs. *Mass* Relation

Finally, we recall that [Goudfrooij et al., 2014] found a correlation between present cluster mass, or escape velocity and age spread, shown in Figure 1.2.4. Since I proved that

rotation is the main responsible of the pseudo-age spread, and clusters are consistent with not-hosting multiple stellar generations, that result is now incomprehensible in the light of the rotation scenario. There is no apparent reason in fact for which cluster age spread should correlate with cluster mass.
In Figure 4.3.2 I plotted Δage vs. cluster mass for my dataset, which includes part of that used in [Goudfrooij et al., 2014] and that of [Milone et al., 2018]. The result is, at first sight, in agreement with that of [Goudfrooij et al., 2014] since the two quantities show hints of correlation, with their Spearman coefficient being $r_{spearman} = 0.59$.

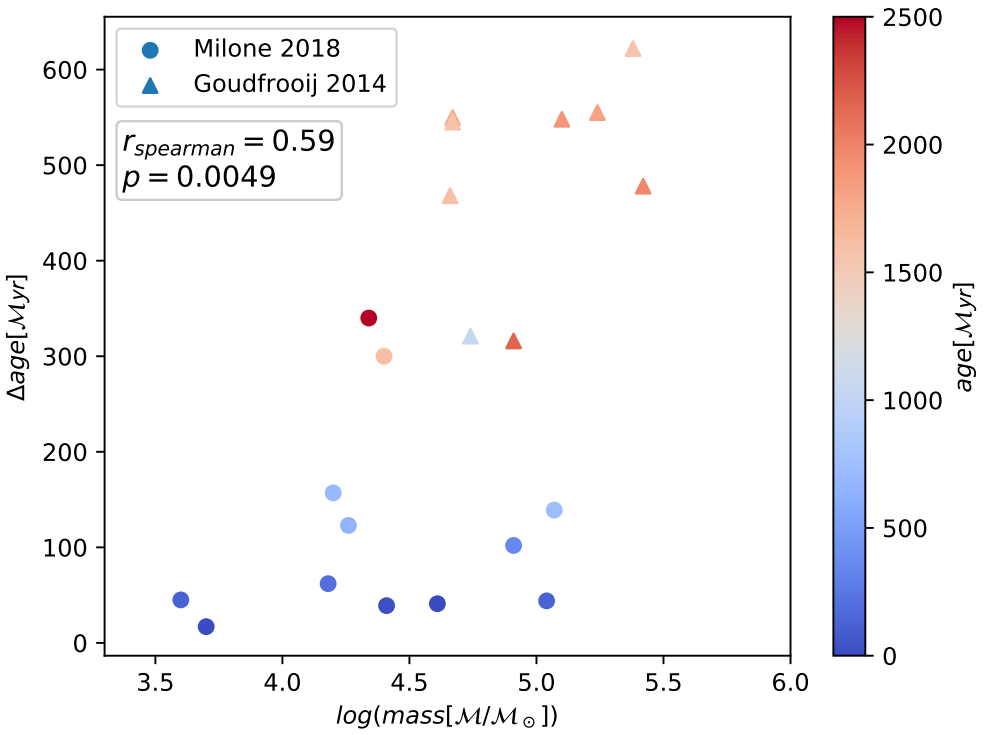

Figure 4.3.2: Same as figure 1.2.4 for present day cluster mass. Filled triangles are clusters whose mass has been taken from [Goudfrooij et al., 2014], while black dots are clusters taken from [Milone et al., 2018]. The color coding represents cluster age, as shown by the colorbar.

One possible explanation is that, for some still unknown reasons, these two quantities correlates, and there is a physical reason behind that. However, another hypothesis is that this correlation is not physical, but it is due to this particular dataset, and is therefore fallacious. I show in Figure 1.2.4 the analysis supporting this hypothesis. First, the Goudfrooij dataset is composed only of cluster older than 1 Gyr (shown as filled triangles), while that of Milone only of clusters younger than 1 Gyr (filled dots). Points are plotted with different color depending on their age, as shown by the colorbar. We see that there is a net division in mass range between older clusters (red shades) and younger clusters (blue shades), in the sense that older clusters have larger masses than younger clusters. Therefore, in the light of the linear dependence of the age spread with cluster age (see Figure 4.2.1), it is natural to find that older (and more massive) clusters have a larger age spread than younger (and less massive) clusters. In other words cluster mass becomes somehow a proxy of cluster age, thus creating the shallow correlation between age spread and mass.

4.4 Summary and Conclusions

In this work I analyzed the CMDs of a large sample of Young and Intermediate-age star clusters in the Large and Small Magellanic Cloud to constrain the physical mechanism that is responsible for the occurrence of Multiple Stellar Populations.

I reduced archive images collected with the wide-field channel of the advanced camera for survey on board of the Hubble Space Telescope and derived high-precision photometry and astrometry of KMHK 250 in the LMC and NGC 265 in the SMC. These two clusters have never been investigated in the context of the multi-population phenomenon.
I discovered that NGC 265 exhibits a split MS and an eMSTO. This fact corroborates the evidence that multiple sequences are a common feature in the CMDs of young star clusters of the Magellanic Clouds. Moreover, I detected an eMSTO in KMHK 250, which is a very sparse low-mass cluster of the LMC. The similarity of the eMSTO in massive clusters and in KMHK 250 demonstrates that the occurrence of multiple populations in intermediate-age clusters does not depend on the cluster mass.

To extend the study to a large sample of GCs, I exploited the photometric and astrometric catalogs of 27 clusters from the HST survey of multiple stellar populations in the Magellanic Clouds. I compared the CMDs with isochrones from the Padova database and estimated the cluster ages, distances, and reddenings. I assumed that age is responsible for the eMSTO and calculated the age spread that is needed to reproduce the observations.
I find that the resulting age spread correlates with the cluster age. Simulated CMDs derived from Geneva models that account for rotation reveal that such trend is consistent with coeval stellar populations with different rotation. Further investigation is needed to understand the physical mechanism that is responsible for multiple populations with different rotation rotation rates within each cluster. Nevertheless, my results provide precious observational constraints to understand the rotational evolution in cluster's stars.
As a consequence, I can claim that none of these clusters has sustained a prolonged star-formation with a duration of more than 100 Myrs, in contrast with conclusions from literature papers. My results suggest that the multiple populations in old GCs and in young and intermediate-age Magellanic-Cloud clusters are due to different physical phenomena.

Bibliography

[Anderson and Bedin, 2010] Anderson, J. and Bedin, L. R. (2010). An empirical pixel-based correction for imperfect cte. i. hst's advanced camera for surveys. *Publications of the Astronomical Society of the Pacific*, 122(895):1035.

[Anderson and King, 2000] Anderson, J. and King, I. R. (2000). Toward high-precision astrometry with wfpc2. i. deriving an accurate point-spread function. *Publications of the Astronomical Society of the Pacific*, 112(776):1360.

[Anderson and King, 2006] Anderson, J. and King, I. R. (2006). Psfs, photometry, and astrometry for the acs/wfc. *ACS Instrument Science Report*, 1.

[Anderson et al., 2008] Anderson, J., King, I. R., Richer, H. B., Fahlman, G. G., Hansen, B. M., Hurley, J., Kalirai, J. S., Rich, R. M., and Stetson, P. B. (2008). Deep advanced camera for surveys imaging in the globular cluster ngc 6397: reduction methods. *The Astronomical Journal*, 135(6):2114.

[Bastian and De Mink, 2009] Bastian, N. and De Mink, S. (2009). The effect of stellar rotation on colour–magnitude diagrams: on the apparent presence of multiple populations in intermediate age stellar clusters. *Monthly Notices of the Royal Astronomical Society: Letters*, 398(1):L11–L15.

[Baume et al., 2007] Baume, G., Carraro, G., Costa, E., Méndez, R., and Girardi, L. (2007). Extended star formation history of the star cluster ngc 2154 in the large magellanic cloud. *Monthly Notices of the Royal Astronomical Society*, 375(3):1077–1086.

[Bertelli et al., 2003] Bertelli, G., Nasi, E., Girardi, L., Chiosi, C., Zoccali, M., and Gallart, C. (2003). Testing intermediate-age stellar evolution models with vlt photometry of large magellanic cloud clusters. iii. padova results. *The Astronomical Journal*, 125(2):770.

[Brandt and Huang, 2015] Brandt, T. D. and Huang, C. X. (2015). Rotating stellar models can account for the extended main-sequence turnoffs in intermediate-age clusters. *The Astrophysical Journal*, 807(1):25.

[Chiosi and Vallenari, 2007] Chiosi, E. and Vallenari, A. (2007). Three clusters of the smc from acs/wfc hst archive data: Ngc 265, k 29 and ngc 290 and their field population. *Astronomy & Astrophysics*, 466(1):165–179.

[Cottrell and Da Costa, 1981] Cottrell, P. and Da Costa, G. (1981). Correlated cyanogen and sodium anomalies in the globular clusters 47 tuc and ngc 6752. *The Astrophysical Journal*, 245:L79–L82.

[De Mink et al., 2009] De Mink, S., Pols, O., Langer, N., and Izzard, R. (2009). Massive binaries as the source of abundance anomalies in globular clusters. *Astronomy & Astrophysics*, 507(1):L1–L4.

[Denissenkov et al., 2015] Denissenkov, P., VandenBerg, D., Hartwick, F., Herwig, F., Weiss, A., and Paxton, B. (2015). The primordial and evolutionary abundance variations in globular-cluster stars: a problem with two unknowns. *Monthly Notices of the Royal Astronomical Society*, 448(4):3314–3324.

[Denissenkov and Hartwick, 2013] Denissenkov, P. A. and Hartwick, F. (2013). Supermassive stars as a source of abundance anomalies of proton-capture elements in globular clusters. *Monthly Notices of the Royal Astronomical Society: Letters*, 437(1):L21–L25.

[D'Ercole et al., 2010] D'Ercole, A., D'Antona, F., Ventura, P., Vesperini, E., and McMillan, S. L. (2010). Abundance patterns of multiple populations in globular clusters: a chemical evolution model based on yields from agb ejecta. *Monthly Notices of the Royal Astronomical Society*, 407(2):854–869.

[D'Antona et al., 2017] D'Antona, F., Milone, A. P., Tailo, M., Ventura, P., Vesperini, E., and Di Criscienzo, M. (2017). Stars caught in the braking stage in young magellanic cloud clusters. *Nature Astronomy*, 1(8):0186.

[Goudfrooij et al., 2017] Goudfrooij, P., Girardi, L., and Correnti, M. (2017). Extended main-sequence turn-offs in intermediate-age star clusters: Stellar rotation diminishes, but does not eliminate, age spreads. *The Astrophysical Journal*, 846(1):22.

[Goudfrooij et al., 2014] Goudfrooij, P., Girardi, L., Kozhurina-Platais, V., Kalirai, J. S., Platais, I., Puzia, T. H., Correnti, M., Bressan, A., Chandar, R., Kerber, L., et al. (2014). Extended main sequence turnoffs in intermediate-age star clusters: a correlation between turnoff width and early escape velocity. *The Astrophysical Journal*, 797(1):35.

[Mackey and Broby Nielsen, 2007] Mackey, A. and Broby Nielsen, P. (2007). A double main-sequence turn-off in the rich star cluster ngc 1846 in the large magellanic cloud. *Monthly Notices of the Royal Astronomical Society*, 379(1):151–158.

[Marigo et al., 2017] Marigo, P., Girardi, L., Bressan, A., Rosenfield, P., Aringer, B., Chen, Y., Dussin, M., Nanni, A., Pastorelli, G., Rodrigues, T. S., et al. (2017). A new generation of parsec-colibri stellar isochrones including the tp-agb phase. *The Astrophysical Journal*, 835(1):77.

[Marino et al., 2008] Marino, A., Villanova, S., Piotto, G., Milone, A., Momany, Y., Bedin, L., and Medling, A. (2008). Spectroscopic and photometric evidence of two stellar populations in the galactic globular cluster ngc 6121 (m 4). *Astronomy & Astrophysics*, 490(2):625–640.

[Martocchia et al., 2018] Martocchia, S., Niederhofer, F., Dalessandro, E., Bastian, N., Kacharov, N., Usher, C., Cabrera-Ziri, I., Lardo, C., Cassisi, S., Geisler, D., et al. (2018). The search for multiple populations in magellanic cloud clusters iv: Coeval multiple stellar populations in the young star cluster ngc 1978. *Monthly Notices of the Royal Astronomical Society*.

[Milone et al., 2009] Milone, A., Bedin, L., Piotto, G., and Anderson, J. (2009). Multiple stellar populations in magellanic cloud clusters-i. an ordinary feature for intermediate age globulars in the lmc? *Astronomy & Astrophysics*, 497(3):755–771.

[Milone et al., 2015a] Milone, A., Bedin, L., Piotto, G., Marino, A., Cassisi, S., Bellini, A., Jerjen, H., Pietrinferni, A., Aparicio, A., and Rich, R. (2015a). Multiple stellar populations in magellanic cloud clusters–iii. the first evidence of an extended main

sequence turn-off in a young cluster: Ngc 1856. *Monthly Notices of the Royal Astronomical Society*, 450(4):3750–3764.

[Milone et al., 2016a] Milone, A., Marino, A., D'Antona, F., Bedin, L., Da Costa, G., Jerjen, H., and Mackey, A. (2016a). Multiple stellar populations in magellanic cloud clusters–iv. the double main sequence of the young cluster ngc 1755. *Monthly Notices of the Royal Astronomical Society*, 458(4):4368–4382.

[Milone et al., 2016b] Milone, A., Marino, A., D'Antona, F., Bedin, L., Piotto, G., Jerjen, H., Anderson, J., Dotter, A., Criscienzo, M. D., and Lagioia, E. (2016b). Multiple stellar populations in magellanic cloud clusters–v. the split main sequence of the young cluster ngc 1866. *Monthly Notices of the Royal Astronomical Society*, 465(4):4363–4374.

[Milone et al., 2018] Milone, A., Marino, A., Di Criscienzo, M., D'Antona, F., Bedin, L., Da Costa, G., Piotto, G., Tailo, M., Dotter, A., Angeloni, R., et al. (2018). Multiple stellar populations in magellanic cloud clusters–vi. a survey of multiple sequences and be stars in young clusters. *Monthly Notices of the Royal Astronomical Society*, 477(2):2640–2663.

[Milone et al., 2015b] Milone, A., Marino, A., Piotto, G., Renzini, A., Bedin, L., Anderson, J., Cassisi, S., D'Antona, F., Bellini, A., Jerjen, H., et al. (2015b). The hubble space telescope uv legacy survey of galactic globular clusters. iii. a quintuple stellar population in ngc 2808. *The Astrophysical Journal*, 808(1):51.

[Milone et al., 2016c] Milone, A., Piotto, G., Renzini, A., Marino, A., Bedin, L., Vesperini, E., D'Antona, F., Nardiello, D., Anderson, J., King, I., et al. (2016c). The hubble space telescope uv legacy survey of galactic globular clusters–ix. the atlas of multiple stellar populations. *Monthly Notices of the Royal Astronomical Society*, 464(3):3636–3656.

[Mucciarelli et al., 2011] Mucciarelli, A., Cristallo, S., Brocato, E., Pasquini, L., Straniero, O., Caffau, E., Raimondo, G., Kaufer, A., Musella, I., Ripepi, V., et al. (2011). Ngc 1866: a milestone for understanding the chemical evolution of stellar populations in the large magellanic cloud. *Monthly Notices of the Royal Astronomical Society*, 413(2):837–851.

[Niederhofer et al., 2015] Niederhofer, F., Georgy, C., Bastian, N., and Ekström, S. (2015). Apparent age spreads in clusters and the role of stellar rotation. *Monthly Notices of the Royal Astronomical Society*, 453(2):2070–2074.

[Ventura et al., 2001] Ventura, P., D'Antona, F., Mazzitelli, I., and Gratton, R. (2001). Predictions for self-pollution in globular cluster stars. *The Astrophysical Journal Letters*, 550(1):L65.

[Yong et al., 2005] Yong, D., Carney, B. W., and de Almeida, M. L. T. (2005). Elemental abundance ratios in stars of the outer galactic disk. i. open clusters. *The Astronomical Journal*, 130(2):597.